3D Printed Patient Specific Surgical Guide for Spine Registration During Minimally Invasive Surgery

Iffa Hujaleh

A thesis submitted to the University of Ottawa
in partial fulfillment of the requirements for the degree of

MASTER OF APPLIED SCIENCE
in
Biomedical Engineering

Ottawa Carleton Institute for Biomedical Engineering

University of Ottawa

Abstract

Minimally invasive spine surgery (MISS) has proven to be advantageous over traditional open surgery as it minimizes the likelihood of tissue damage and infections. During MISS, surgeons create small incisions to allow access to the surgery site, however, opting for smaller incisions decreases the surgeon's field of vision. To compensate, surgeons rely on preoperative and intraoperative ionizing imaging technologies for guidance.

Conventional localization of the spine, registration of digital images to the patient during surgery, depends heavily on the surgeon's anatomical knowledge and their experience. Preoperative images are typically created using 3D technology while intraoperative images use 2D technology. While the integration of preoperative 3D images and intraoperative 2D images can provide valuable assistance, patient's preoperative and intraoperative positions do not coincide leading to additional use of ionizing imaging.

The objective of this research was to propose a workflow that assists with image registration for MISS. The main component of the workflow was the creation of a script that automatically generates patient-specific digital guides, which will then be manufactured, to align the patient's intraoperative and preoperative body position. By aligning the patient's positions, the 3D printed surgical guide serves as a shared feature between the preoperative digital image and the actual patient. This allows for the intraoperative image to be registered to the preoperative image more accurately. Additionally, the guide acts as an attachment site for any additional instrument guides/supports.

The surgical guide generating script utilizes the skin contour of patient's torso region, extracted from medical images, to automatically produce the guide's horizontal and vertical components. Adjustments are made to the components using CAD software before proceeding to manufacturing, via 3D printing, and assembly of the guide. To validate the workflow, more

specifically the script's ability to automatically generate surgical guides that fit over the patient's back, a guide was created for a mannequin. The maximum gap between the mannequin and the horizontal components was 0.8 cm and 1.5 cm for the vertical component.

Acknowledgment

First and foremost, I would like to thank God for enabling me to successfully complete my master's degree and surrounding me with supportive people during these trying times.

There are many individuals I would like to thank who assisted me in reaching my goals and completing this thesis.

I would like to especially thank my supervisor, professor WonSook Lee for her endless support, encouragement, and insightful suggestions. This journey would be difficult without her. Being a part of her lab was a privilege. I learnt a lot and met an incredible group of people. I would particularly like to thank Jiawei Li whose work informed my research.

I would also like to thank the Makerspace staff for allowing me to access equipment, which were difficult to come by, during this pandemic.

Last, but definitely not least, I would like to thank my family (Hoyoo, Hafsah, Filsan, Rachida, Amayah, Koshin, Hamda, Hersi, Adeero, and Ali) and friends (Sereen and Noor) for constantly cheering me on, pushing me and providing me with their support.

Dedication

To my hoyoo macaan

Table of Contents

List of Figures

List of Tables

List of Abbreviations

2D	Two-dimensional
3D	Three-dimensional
ABS	Acrylonitrile butadiene styrene
CAD	computer-aided design
CT	Computer tomography
DRO	Dynamic rigid object
FDM	fused deposition modeling
MISS	Minimally invasive spine surgery
MJM	MultiJet modeling
MRI	Magnetic Resonance imaging
PETG	Polyethylene terephthalate
PLA	Polylactic acid
SLA	Stereolithography
SLS	Selective laser sintering
TE	Echo time
TPE	thermoplastic elastomer
TPU	Thermoplastic polyurethane
TR	Repetition time
PLIF	posterior lumbar interbody fusion
TLIF	transforaminal lumbar interbody fusion

Chapter 1: Introduction

In our 21st century society, there is a strong emphasis and value placed on innovation and technological advancements. Innovative techniques and new technology are constantly being introduced in the field of medicine. Although this is the case, certain medical fields, such as surgery, are steeped in a proud history of science and traditions, and, as a result, have been slow to adopt new ways of doing things. Despite this, rapid developments in technology, research and a shift to a patient-centric approach in medicine have led to reappraisals of long-standing procedures performed in the operating room. In recent years, there seems to be more openness to the adoption and use of new surgical procedures, especially ones that are proven to be effective and less invasive [1]. Spine surgery, in particular, has evolved significantly and continues to as more research and technological advancements are made [2].

Traditionally, spine surgery has been performed as an open procedure (Figure 1 (a)), where surgeons make a large incision allowing for direct access to the spine. The main concern regarding large incisions is the increased likelihood of patients suffering from tissue damage and infections, due to the extensive dissection of soft tissue [3]–[7]. Most patients that undergo open procedures experience muscle trauma and are required to remain hospitalized for a longer duration [8]. An alternative approach which revolutionized spine surgeries and minimized the collateral damage associated with open procedures is minimally invasive spine surgery (MISS) (Figure 1 (b)).

MISS procedures have been proven to be advantageous over open surgery [9]–[12]. Smaller incision(s) are made, which limits damage made to surrounding soft tissues and wound-related complications [13], [14]. More specifically, in comparison to open procedure, small incisions decrease the likelihood of skin dehiscence and postoperative contamination [15]. MISS also decreases the chances of sustaining infections and the recovery period [16]. These benefits, taken together, reduce the cost of treating spine disease, while addressing the problem at hand [16].

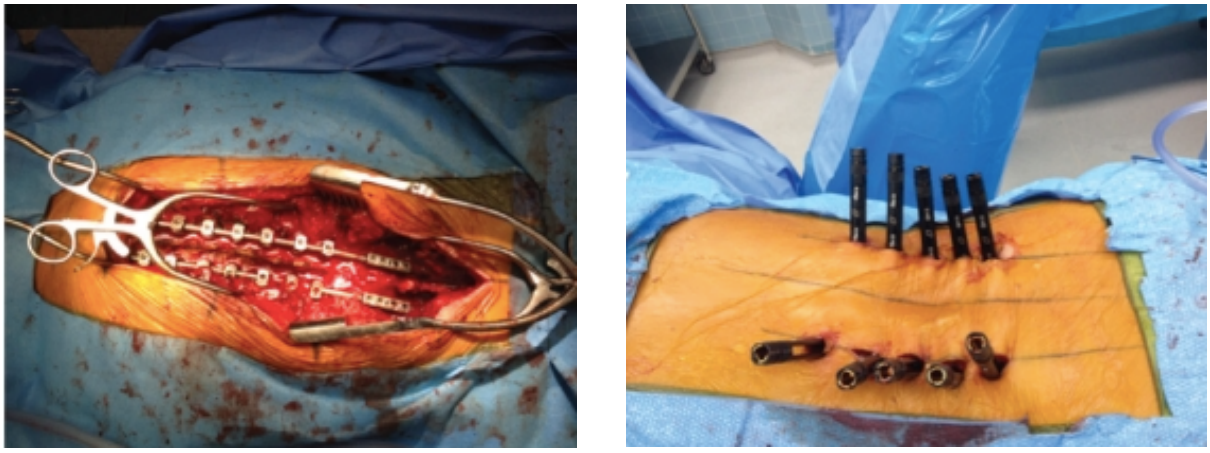

Figure 1 (a) Open spine surgery (b) Minimally invasive spine surgery (Reprinted from [17])

1.1 Problem Statement

Despite the several advantages associated with MISS, the learning curve is relatively steep especially for surgeons who are accustomed to performing open procedures [18][2][19]. Surgeons must become accustomed to unfamiliar tools and technology. Other challenges presented by MISS include: a decreased field of vision, a lack of tactile sensation, and a need for a high level of manual dexterity [2], [20], [21]. Due to the limited exposure of anatomical landmarks, intraoperative imaging becomes indispensable for accurate placement of surgical instruments [22], [23].

When it comes to MISS, C-arm fluoroscopy is the most commonly used intraoperative imaging technology—it provides rapid and serial visualization of two-dimensional (2D) images in real time [24] [25]. C-arm fluoroscopy is able to guide surgeons accurately in level verification and placement of spinal instrumentation [26]. Furthermore, it is highly mobile, widely available, and low cost. However, C-arm fluoroscopy exposes patients and medical staff to a high level of radiation, it is limited to 2D imaging in a single plane at a time, and it has a higher error rate for instrument placement compared to three-dimensional (3D) imaging [25], [27], [28].

In addition to preoperatively acquired 3D images, namely computer tomography (CT) and/or magnetic resonance imaging (MRI), traditional spinal localization technique relies on the surgeon's knowledge of the anatomy and experience and is supported by intraoperative fluoroscopy [29]. The integration of preoperative 3D images and intraoperative 2D images can provide valuable assistance, however, the issue of image content mismatch arises which can pose challenges for image-based registration. The discrepancy between intraoperative and preoperative patient position is among the sources that cause content mismatch [30], [31]. Technologies such as intraoperative imaging technologies, navigation systems, and 3D printed guides have been developed to improve accuracy of tool and hardware placements and to reduce radiation [32]. While navigation systems improve accuracy, any shift in body position requires re-registration, increasing radiation exposure.

In clinical settings across various disciplines, 3D printing has been employed for surgical purposes, including fabrication of biomodels for preoperative planning, intraoperative surgical templates, and intraoperative guidance devices [33], [34]. As stated by Hsu et al. [35], the ultimate goal of 3D printing as a guiding instrument for MISS would be to construct a device that fits externally on the patients' body that guides drill trajectory and placement of screws without invasive exposure.

The objective of this research was to propose a workflow that assists with image registration for MISS. The main component of the workflow was the creation of a script that automatically generates digital patient specific guides, that is solid, to align the patient's intraoperative and preoperative body position. By aligning the patient preoperative and intraoperative body positions, the 3D printed surgical guide serves as a shared feature between the digital images and the actual patient. Additionally, the guide acts as an attachment site for any additional instrument guides/supports.

1.2 Proposed Surgical Process Model

While this research focuses on registration between preoperative and intraoperative imaging, the ultimate aim of this research is promoting the elimination of radiation when MISS is performed. This research illustrates how fixed axis-controlled imaging, C-arm fluoroscopy, can be replaced with the integration of safer free-hand imaging, ultrasound, preoperative MRI and a surgical guide. Intraoperative ultrasound remains to be the only true real-time and radiation-free image modality to continuously visualize soft tissue during surgery [36]. However, as one of the first imaging modalities discovered, ultrasound suffers from major limitation: a lack of orientation and panoramic view. Due to these shortcomings, knowing where to place the ultrasound probe can take some time. To overcome this shortcoming, MRI and ultrasound image fusion is an area that requires exploration [37].

Figure 2 provides an overview view of the proposed process. Preoperative images are first acquired to begin the process. Once the images are preprocessed, they will be used for preoperative planning which entails creating a biomodel of the patient's spine, creating a patient specific surgical guide, and planification of surgical instruments and tools trajectory. The purpose of the surgical guide is to match the patients preoperative and intraoperative body position. The guide can also assist physicians in determining where to place surgical tools (i.e. ultrasound probe and tubular retractors). Figure 3 displays the setup of the surgical guide with the ultrasound probe and tubular retractor(s) guides attached.

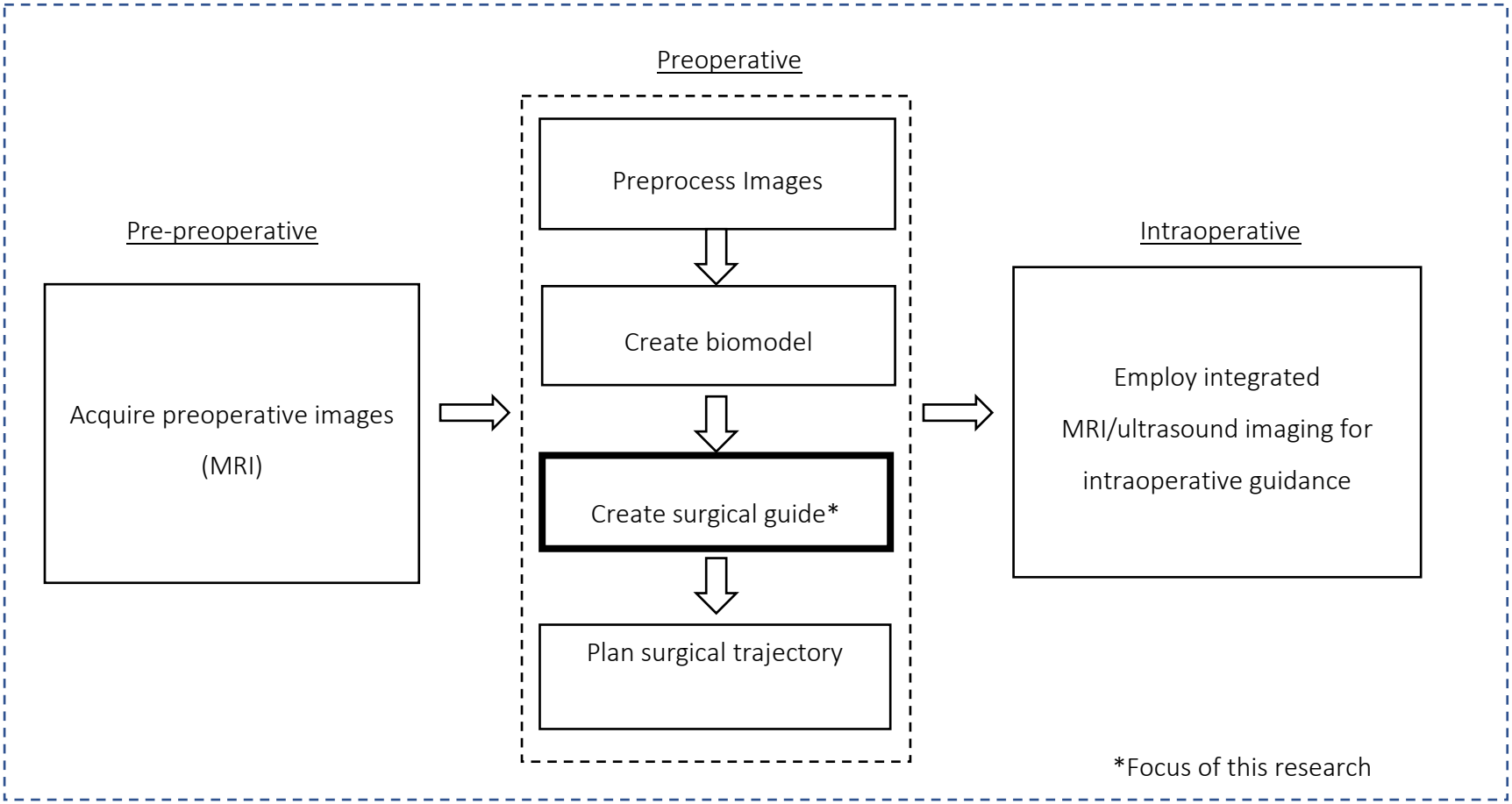

Figure 2 Overview of Concept: (1) preoperative images are acquired. (2) Preoperative planning occurs by creating biomodel and surgical guide, and planning trajectory of tools. (2) Intraoperative ultrasound is used for surgical guidance once integrated with preoperative MRI images

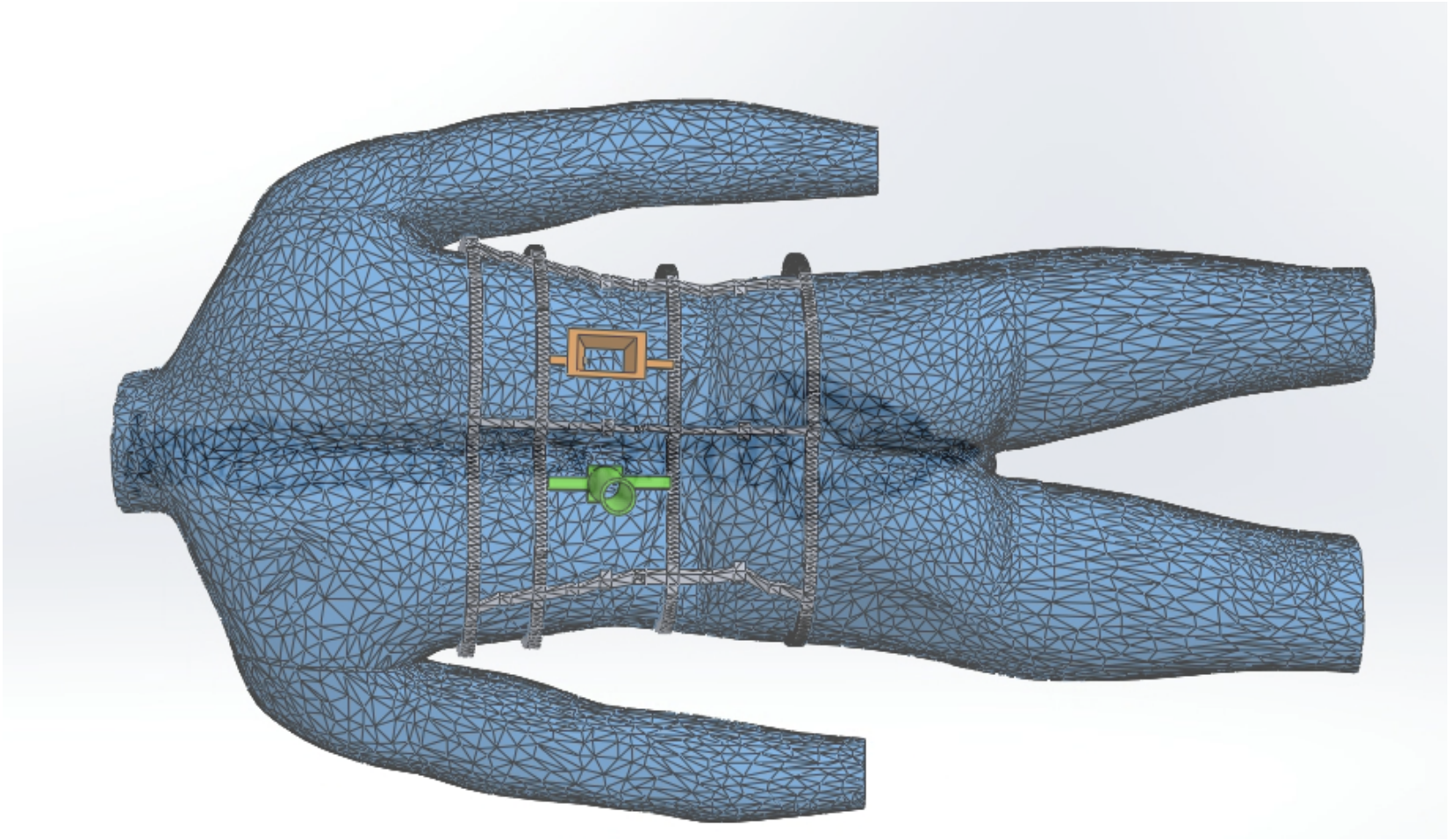

Figure 3 Setup example of surgical guide with tubular retractor (green) and ultrasound probe (orange) guides attached

1.3 Contribution

The main contribution made by this thesis is the proposal of a new method—using a 3D printed surgical guide, to help align preoperative and intraoperative imaging. The details of the process include:

1. Development of an image registering method for MISS
2. Development of a clinical workflow for the fabrication of surgical guides
3. Development of a surgical guide used to assist with accurate alignment and placement of surgical tools
4. Development of a surgical guide that serves as a shared feature between digital and actual patient

1.4 Thesis Outline

Chapter 2 provides an overview of spinal anatomy and pathology, a brief review of MISS techniques, an overview of imaging technology used for spine surgery, and a literature review of 3D printed image registering assisting guides. The following chapter (chapter 3) outlines the method employed to create the surgical guide. The results and validation of the proposed workflow is then discussed in Chapter 4 and 5 respectively. A discussion of the results is provided in chapter 6. Lastly, chapter 7 briefly summaries the main conclusions of this research, study limitations and future research that can be carried in this research domain.

Chapter 2: Background

2.1 Spinal Anatomy

The spine, also known as the vertebral column or spinal column, is a complex structure consisting of 26 irregular bones, vertebrae, which are held together with ligaments and muscles extending from the neck to the pelvis [38]. The purpose of the spine is to provide support to the body, while allowing movement, and protection of the spinal cord which continuously carries signals back and forth between the brain and the peripheral nerves [38], [39]. Vertebrae are connected to each other in a flexible manner creating a curved structure (
Figure 4). A healthy spine takes the form of a S-shaped curve in order to maintain balance of the body and support its weight [40]. The curvature of the spine can be divided into 5 main regions: the cervical curvature, the thoracic curvature, the lumbar curvature, the sacral curvature, and the coccyx. The cervical and sacral vertebrae concave anteriorly while the thoracic and sacral vertebrae convex anteriorly. The cervical curvature comprises of 7 vertebrae (C1-C7), the thoracic curvature 12 vertebrae (T1-T12), and the lumbar curvature 5 vertebrae (L1-L5). The sacral curvature consists solely of the sacrum. Both the sacrum and coccyx are formed from fused vertebrae, 5 and 4 vertebrae respectively [41]. To prevent rubbing and to absorb pressure, intervertebral discs are located in between unfused adjacent vertebrae.

Intervertebral discs are composed of two components, the nucleus pulposus and the annulus fibrosus. The nucleus pulposus is a jelly like material that allows the vertebrae disc to resist compression and torsion forces. The annulus fibrosus surrounds the nucleus pulposus and bridges the gap between adjacent vertebrae [42].

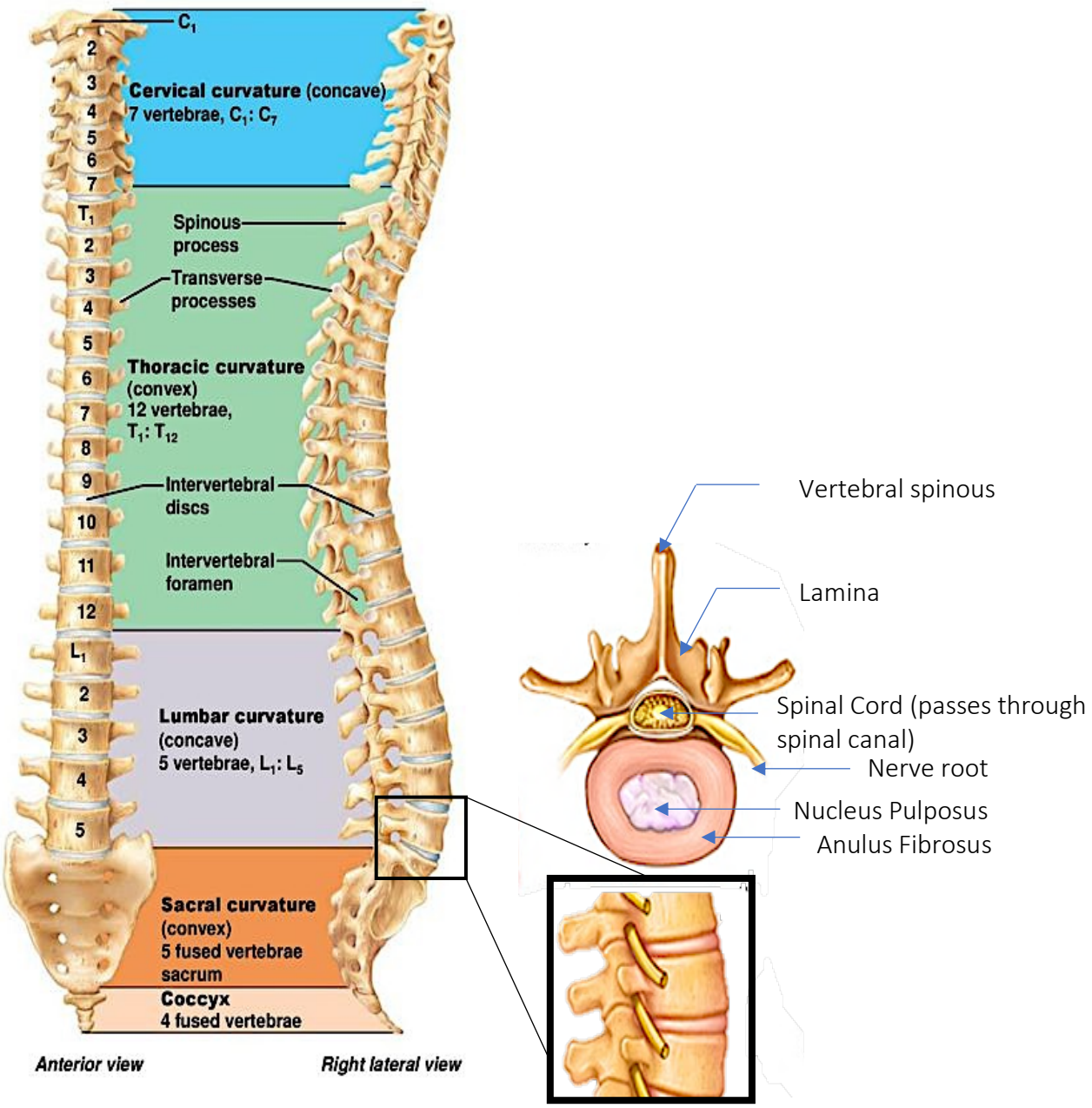

Figure 4 Spinal curvature Spinal nerve

(Adapted from [38]*)*

2.2 Treatment of the Spinal Disorders

Spinal disorders are initially treated with conservative approaches such as physical therapy, pain medication and steroid injections to relieve pain, restore function, and improve quality of life [43]. After exhausting all possible non-surgical options, or the condition is complex, treatments will lead to surgical intervention [44]. Notwithstanding etiologic factors (e.g. trauma, degenerative conditions, neoplasm, etc.) relating to spine conditions, effective surgical management of spinal pathology can be simplified into two concepts, decompression and stabilization. Compression of the spinal cord and/or nerve roots can lead to neurological deficit while spinal instability can cause pain and deformity resulting in neurological impairment. The type of treatment chosen for a given spinal condition is determined by the location, level of pathology, and the surgeon's experience [45]. A given condition is not restricted to a single procedure. For example, surgical procedure for lumbar disc disease includes discectomy, posterior lumbar interbody fusion (PLIF), transforaminal lumbar interbody fusion (TLIF), and surgical procedure for lumbar spinal stenosis and spondylolisthesis includes laminectomy, PLIF, and TLIF.

2.2.1 Laminectomy and Discectomy

Laminectomy and discectomy are both decompressive procedures that release pressure applied to the nerve or spinal cord. While laminectomy decompresses the spine by removing the lamina, discectomy decompresses the spine by removing the portion of the disc compressing the nerve. Conventionally, laminectomy is performed in an open manner which includes dissection of spinal muscles to access the lamina (Figure 5 (a)) [46]. Minimally invasive approaches have allowed laminectomy to be performed while keeping soft tissues intact (Figure 5 (b)).

(a) (b)

Figure 5 (a) Open laminectomy, (b) minimally invasive laminectomy ((Reprinted from [47]*)*

Traditional discectomy requires performing a laminectomy first to gain access to herniated discs. In addition to the removal of laminae, nerve roots are retracted, and ligaments are removed. (Figure 6 (a)) [48]. Excessive removal of bone can lead to instability thus requiring stabilization. Arthroscopically assisted microdiscectomy is a commonly performed minimally invasive alternative that does not require muscle stripping, bone resection, or retraction of nerve roots (Figure 6 (b)). This percutaneous procedure uses fluoroscopic guidance to direct surgeons to the triangle working zone to remove the disc fragments causing the impingement [49].

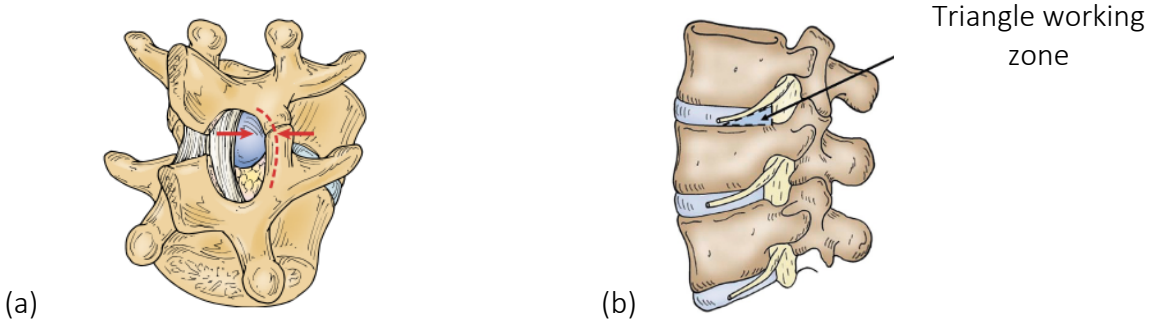

(a) (b)

Figure 6 (a) Conventional discectomy: removal of laminae and ligament to expose pitched nerve and remove herniated disc.(b) Percutaneous arthroscopic discectomy: removal of disc fragment via the triangle working zone (Reprinted from [50], [51]*)*

2.2.2 Posterior Lumbar Interbody Fusion (PLIF)/Transforaminal Lumbar Interbody Fusion (TLIF)

Spinal fusion is commonly performed to address instability or problems related to spinal alignment. The goal of spinal fusion is to achieve a solid arthrodesis of spinal segments, restore disk height, immobilize unstable segments, and restore load bearing to anterior structure [52]. PLIF and TLIF are two fusion procedures performed to manage lumbar spinal disorder that require arthrodesis. PLIF involves the removal of the lamina and facets on both side of the vertebrae, while TLIF on one side.

Conventional fusion involves making a midline incision to remove the lamina and superior and inferior facet to the access the spinal canal. Neural elements are then retracted to entirely remove disc. Most fusion procedures include the insertion of structural grafts and an implant into the space that was preoccupied by the disc (Figure 7) [45]. Technological advancement has allowed fusion procedures to be performed in a minimally invasive manner. Minimally invasive TLIF approaches, similar to other minimally invasive surgeries, allows for muscle to remain intact as they are dilated rather than dissected [53], [54].

(a) (b)

Figure 7 Removal of disc (left), insert of graft and implant (Reprinted from [55]*)*

2.2.3 Minimally Invasive Approaches

Various methods have been developed for traditional decompression and stabilization issues, including endoscopic approach, tubular approach, and percutaneous approach [56]. The advantages and disadvantages of each approach are outlined in Table 1 .

Table 1 Strength and shortcomings of minimally invasive techniques (Adapted from [2]*)*

Approach	Advantages	Disadvantages
Percutaneous	• Shorter learning curve in comparison to tubular/endoscopic techniques • Similar to tubular and endoscopic technique, muscle-splitting approach allows minimal soft tissue disruption, faster recovery time, and reduced blood loss	• Small surgical field and narrow window for visualization • Difficult exposure of the central spinal canal for decompression
Tubular	• Working channels tailored to help expand field of visualization • Dilation minimizes trauma to soft tissue • Allows for easy fine tune adjustments in the trajectory of ports compared with endoscopic techniques	• Microscope-assisted operations require co-axial vision • Careful consideration must be made with serial dilation of retractors • Higher learning curve
Endoscopic	• Direct visualization of anatomy with relatively easy shifts in camera angle • Evolving technique with the use of adjunct applications	• Relatively longer operative times • Higher learning curve

The percutaneous approach is similar to open surgery except advanced techniques are used to minimise the size and extent of the incision (Figure 8 (a)). With the advances of visualization and illumination technology, percutaneous procedures have become relatively easy to perform. This approach has become a desirable alternative for surgeons who are accustomed to open procedure. Tubular approach involves the use of tubular retractors which act as an access port to the spine. Before inserting the retractors, dilators are inserted to push aside soft tissues to obtain the desired incision size (Figure 8 (b)). Endoscopic technique requires the use of an endoscope to access the spine (Figure 8 (c)) [18].

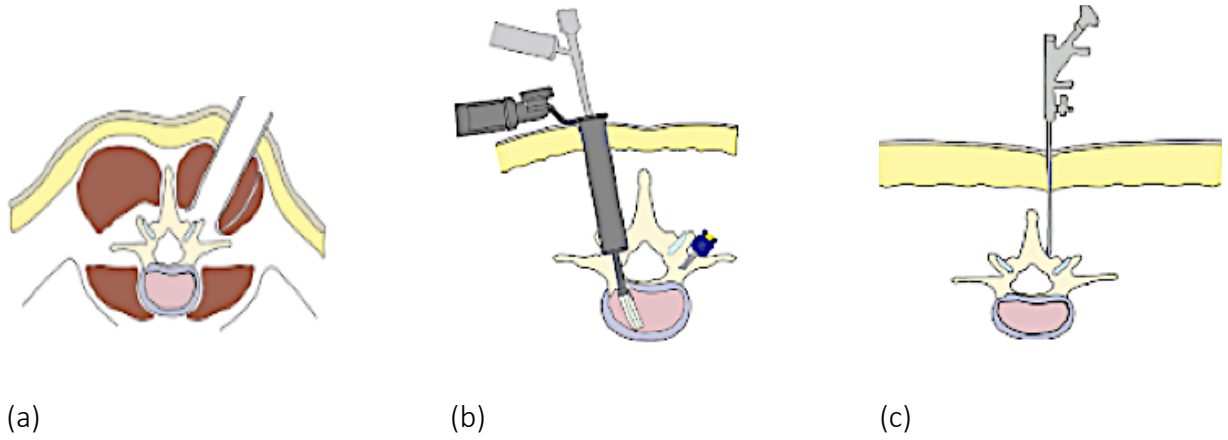

(a) (b) (c)

Figure 8 (a) Percutaneous, (b) tubular, (c) endoscopic (Adapted from: [2]*)*

Among the techniques mentioned above, the tubular technique in particular has altered the paradigm of spine surgery [57]. With the use of tubular retractors, morbidity is decreased and the field of visualization can be expanded while minimizing trauma to soft tissues [58] [59]. The location, number of retractors, and the orientation of tubular retractor is determined by the spinal disorder (Figure 9).

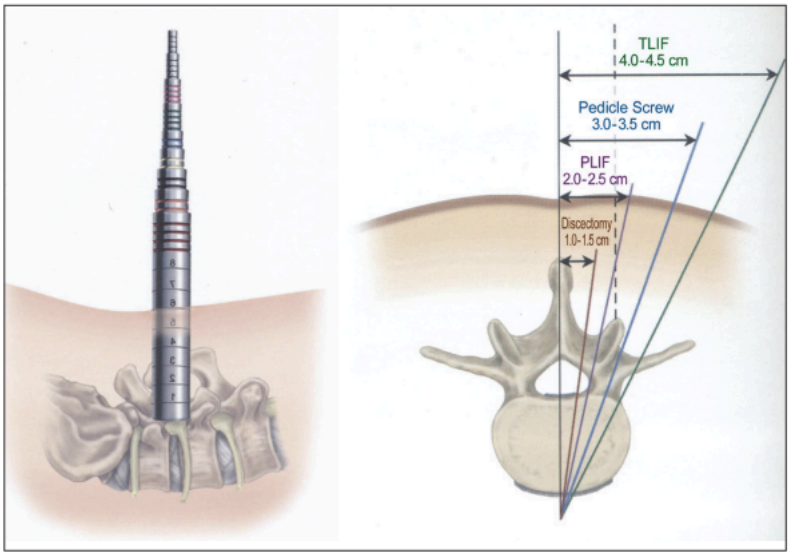

Figure 9 Position of retractor given surgical procedure (Reprinted from [60]*)*

2.3 Imaging Modalities of the Spine

Medical imaging encompasses an array of modalities used to examine the interior of the human body noninvasively. Imaging can be applied for diagnostic, monitoring, and treatment purposes. Selecting the appropriate imaging modality depends on a wide variety of factors including pathology and contraindications [61]. While considering these factors and weighing the strength and limitations of each modality, physicians are able to choose the ideal device for a given case.

The pioneer of image modality, plain radiography (x-ray), is commonly used for evaluating symptoms localized in the spine (e.g. pain, numbness and weakness). Due to its ease in acquisition and cost, x-ray is typically the first choice for diagnostic testing. With x-ray imaging, the stability and flexibility of the spine can be evaluated with the implementation of specialized views [62]. However, plain radiography is unable to identify soft tissues and lacks 3D characteristic. Two modalities in particular that have revolutionized the diagnosis and surgical management of spinal disorder are CT and MRI. These modalities can provide postoperative evaluation, previously unachievable with plain radiography, in addition to providing images of high resolution and 3D

characteristics [63]. Since CT and MRI are unable to capture real-time imaging, using them independently during MISS is not ideal.

2.3.1 Preoperative and Intraoperative Imaging

The limitation of imaging devices and challenges posed by the spine's complex anatomical configuration are two factors that have led to the improvement of existing imaging technology. Imaging technology, as well as navigation systems, have been introduced in spine surgery to decrease radiation exposure and increase instrumentation accuracy [64]. Preoperative CT, intraoperative CT, and 3D fluoroscopy are examples of imaging technology paired with navigation systems.

Preoperative CT images were the basis of the earliest surgical navigation system. These images were acquired using preoperative standard scan protocol [25]. Although preoperative CT based navigation is highly effective, there are notable disadvantages associated with this approach. In experienced hands, the registration process may appear relatively straightforward, however, selecting the anatomic landmarks and matching the image anatomy involves a significant learning curve. Since the position of the patient is commonly different before and during surgery, intersegmental relationship between neighbouring vertebral levels may also be different [65]. Additionally, this technique is time consuming because each vertebra needs to be registered individually, and re-registered when anatomy shifts during surgery [66].

Intraoperative 3D imaging addresses concerns related to navigational inaccuracy caused by the difference in intervertebral alignment between preoperative images and intraoperative patient position [25]. Two intraoperative 3D imaging currently implemented in navigation systems are Intraoperative CT and 3D fluoroscopy. Each device technique has its advantages and disadvantages as outlined in Table 2. Using CT scanner intraoperatively is restricting as it requires the use of integrated tables posing logistic and scheduling challenges [67]. Most

intraoperative 3D imaging chosen for intraoperative navigation is 3D fluoroscopy; they are mobile and more cost efficient.

Table 2 Summary of advantages and disadvantages of intraoperative 3D imaging

Technology	Advantages	Disadvantages
Intraoperative CT	• High resolution • Large field of vision	• Higher cost • Difficult to use across multiple operating rooms • Takes more time
3D Fluoroscopy	• Mobile • Compact unit • Lower cost • Efficient registration • Faster	• Lower image quality • Limited field of vision

2.3.2 Commercially Available Imaging Technology

Among the numerous intraoperative imaging platforms commercially available, the following intraoperative 3D fluoroscopy technologies will be examined: O-arm by Medtronic, CIOS Spine by Siemens, and Vision RFD 3D by Ziehm. These 3D scanners are beneficial when speed is preferred over image quality. Selected specifications of the technologies are displayed in Figure 10 [67]. The cost of these technologies' ranges from $430,000 to $1,000,000, with Medtronic O-arm costing the most. Both the Medtronic O-arm and RFD 3D provides a field of vision of 20 cm while the Siemens CIOS Spin provides 16 cm. Out of the three technologies, Ziehm RFD 3D provides the highest compatibility (i.e., integration with the most navigation systems).

		
Medtronic O-arm	Ziehm RFD 3D	Siemens CIOS Spin
• $600,000-$1,000,000 • Field of vision: 20 cm • Allows longer segments of the spine to be imaged efficiently • Integrates well with Stealth navigation	• $430,000-$480,000 • Field of vision: 20 cm • Highly mobile • Highest compatibility, Integrates with most navigation platforms • Brainlab, Stryker, Medtronic • 2D functionality	• $400,000-$500,000 • Field of vision: 16 cm • Easily mobile • Integrates with BrainLab

Figure 10 Specification of 3D scanners (Adapted from [67]*)*

Intraoperative CT has also been integrated with navigation system providing higher quality images. Currently, there are two devices available: Mobius Airo by BrainLab and BodyTom by Samsung. The specifications of these technologies are shown in Figure 11. Intraoperative CT provides a larger field of vision compared to 3D fluoroscopy. Mobius Airo providing a field of vision of 56 cm and BodyTom 60 cm. However, the cost for intraoperative CT is more than intraoperative 3D—it ranges between $700,000 and $1,200,000.

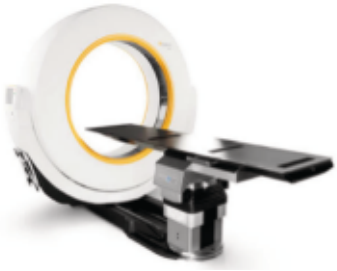

Mobius Airo (BrainLab)

- Cost: $600,000 - $1,200,000
- Field of vision: 57 cm
- Accommodates for large patients
- Possess an assisted drive for movement and an integrated table
- Integrates with BrainLab exclusively
- Basic CT diagnostic and viewing capabilities

Samsung BodyTom

- Cost: $700,000 - $1,100,000
- Field of vision: 60 cm
- Requires a cantilevered carbon fibre table
- Smaller detectors, a more powerful generator, less noise, and software to reduce metal artefacts

Figure 11 Intra-operative CT scanners (Adapted from [67]*)*

2.4 Image-guided Navigation

Typically, image-guided systems, also known as computer-assisted navigation (CAN), consist of a tracking device, tracked tools, and a computer system. Optical tracking cameras are most commonly used as a tracking device [68]. The tracking device continuously monitors the patients

position and the orientation of the tracked tools. Among the tools being tracked, there is a unique instrument called the dynamic rigid object (DRO). The DRO is a tool anchored to the spinous process of a neighbouring vertebra or the iliac crest and serves as a reference point for all other tools being tracked. The position and orientation of the other tools are identified in a coordinate system relative to the DRO. The position and orientation of the tracked tool are inputted into the computer system. A special software manages the tracking of surgical tools, registration of preoperative and/or intraoperative image to the patient, and visualization of tracked tools and registered images. During surgery, the surgical tools and images are rendered and shown on the same screen to display the orientation of the surgical tools relative to the patients anatomy [69].

2.4.1 Commercially Available Navigation Technology

Currently available navigation systems that will be discussed include the BrainLab system by BrainLab, Stealth Station S8 by Medtronic, 7D Surgical System by 7D Surgical, and Stryker Spinal Navigation with Spine Mask by Stryker [70].

The most commonly used navigation platform is the Stealth navigation system. The Stealth navigation system is recommended to be paired with the O-arm. Similar to Medtronic, BrainLab produces both navigation systems and imaging devices. The BrainLab system integrates with a wide range of imaging platforms but its functions are optimized when paired with Airo. The BrainLab system has an automatic registration with Airo intraoperative CT imaging. The navigation system by BrainLab is also compatible with 2D and 3D fluoroscopy, and its surface-matching registration ability allows for the usage of preoperative CT images for navigation.

Unlike other navigation systems, Stryker navigation uses battery powered instruments for tracking. While most navigation platforms require bone anchoring trackers (DRO), Stryker's tracker Spine Mask, consists of an adhesive frame (Figure 12). The SpineMap software allows for intraoperative 3D images to me taken with or without the need to merge them to preoperative CT or MRI images.

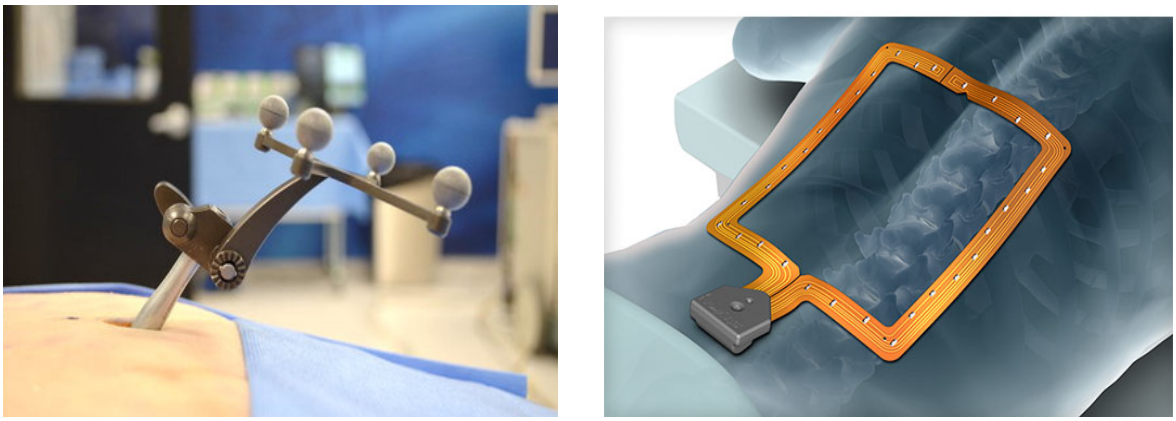

Figure 12 Dynamic reference base (left)), Spine Mask (right)

The 7D surgical system utilizes similar technology to autonomous cars, machine vision. Bony anatomy is co-registered with pre-exiting imaging. In order for registration to occur, direct visualization of bone is required to capture the needed data points. Up to 250 000 data points over an area of 40 cm by 30 cm can be captured. Registration and re-registration, if tracker is displaced, occurs rapidly [67].

Although the use of spinal navigation and imaging technology is favourable, there are a number of factors that could deter their use [71], namely, the cost, lack of necessity, intraoperative interruption, lack of adequate training, difficulty integrating into operating room workflow [72] [73] [74][75][76]. Potential registration error can arise due to the fact that navigation and imaging platforms are separate devices [77].

			
Medtronic Stealth	BrainLab	7D Surgical	Stryker
• $500,000-$700,000 • Passive instrument tracking • Interfaces with iMRI, iCT,C-arm, O-arm • Optical or electromagnetic tracking	• $500,000-$700,000 • Passive instrument tracking • Common imaging devices can be integrated • Third party instrumentation can be visualized	• $400,000-$600,000 • Passive instrument tracking • Open procedure	• $250,000-$450,000 • Active instrument tracking • Only non-invasive tracker (Spine Mask) • Software compatible with third party imaging technology

Figure 13 Specifications of navigation systems available (Adapted from [67]*)*

2.5 3D Printing

3D printing is a manufacturing method that produces objects from a digital computer-aided design (CAD) model. Objects are created by fusing or depositing material such as plastic, metal, ceramic, powder, liquids, or cells through additive manufacturing process [78]. Additively manufactured models are constructed in a layer-by-layer manner [79]–[81]. As oppose to

subtractive manufacturing, the waste produced with additive manufacturing is far less (Figure 14[35].

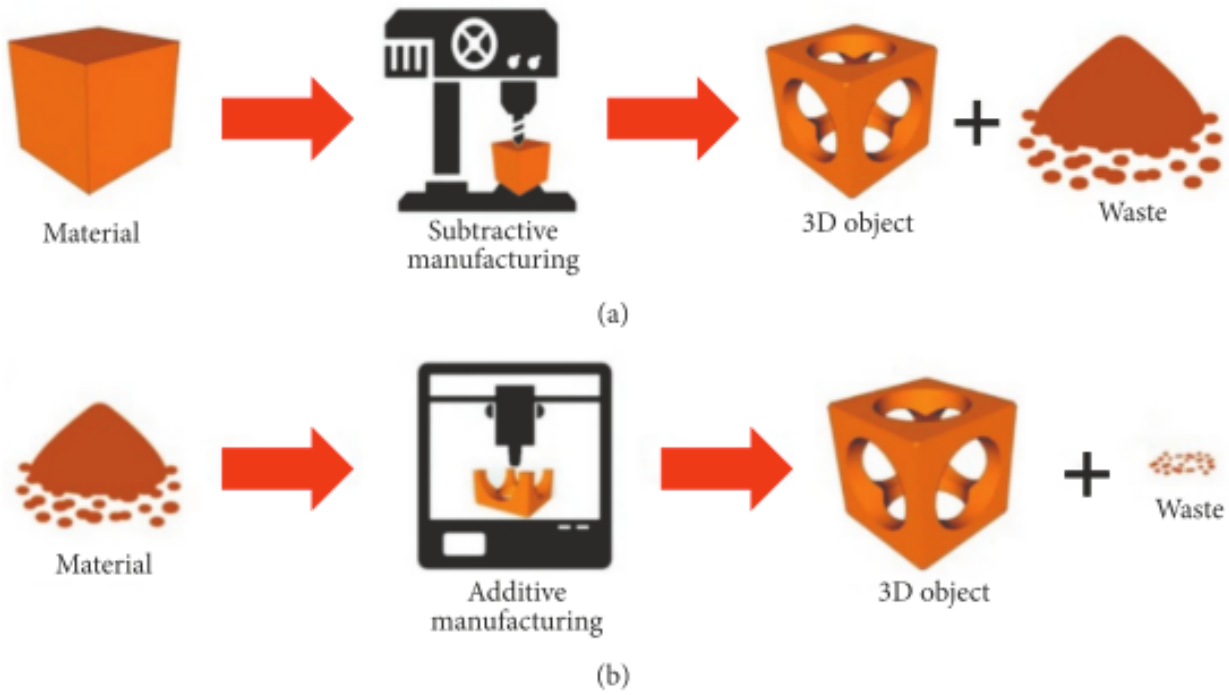

Figure 14 (a) Subtractive manufacturing: process in which material is removed to produce desired shape (b) Additive manufacturing: process in which material is added successively to produce desired shape (Reprinted from [35]*)*

3D printing has been used in industry design since the 1980. Only in recent years has it become adapted for medical applications [82] . The main 3D printing techniques explored in the clinical setting are stereolithography (SLA), MultiJet modeling (MJM), selective laser sintering (SLS), binder jetting, and fused deposition modeling (FDM) [83]. A summary of the advantages and disadvantages of each technique are displayed in Table 3.

Table 3 Summary of the most commonly used 3D printing techniques in medical field application

(Adapted from: [83]*)*

3D Printing Techniques	Advantages	Disadvantages
SLA	• Current gold standard • High resolution • Increased efficiency with increase in print size • Detailed fabrication of internal structure	• More than a day of printing time required • Requires extensive post-production manual handling • High cost
MJM	• High resolution • Minimal post-production manual handling • Multiple materials	• High cost • Poorer surface finishing than SLA
SLS	• Does not require support structures • Smooth surface finishing • Print delicate structures	• Requires post-production manual handling • High cost • Requires expert handling of the printer
BJT	• Does not require support structure • Multiple colours and materials	• Brittle • Require extensive post-production manual handling • Poor surface finish
FDM	• Low cost • Minimal maintenance • High availability of printers	• Requires post-production • Manual removal of support structures • Poor surface finish • Mono-colour and mono-material with the current technology

2.5.1 Medical Application of 3D Printing

The use of 3D printing in the medical field is expanding rapidly. Hospitals, including The Ottawa Hospital, have integrated medical 3D printing programs for surgical planning, education, and research. The benefits of 3D printing in medical applications include: customization and personalization, increased cost efficiency, enhanced productivity, and democratization and collaboration [78] [84] .

The ability to produce custom-made medical products and equipment is the greatest advantage of 3D printing in medical applications. Producing 3D printed devices, such as customized prosthetics and implants , can provide great value to both patient and physician [85] . While it is less expensive to employ traditional manufacturing for large-scale production, cost of 3D printing has become more competitive for small production runs [86]. Manufacturing cost can be reduced by decreasing the use of unnecessary resources when 3D printing [87]. Additionally, 3D printing is much faster than traditional methods and the resolution, accuracy, reliability, and repeatable are improving [85]. In comparison to conventional manufacturing, 3D printing allows for rapid production of customized objects with complex geometries [88]–[91]. 3D printing allows people from all fields, including medicine, to design and produce novel products. The nature of 3D printing files allows for collaboration of researchers [92].

Medical area where 3D printing has been implemented include surgical planning, development and design of devices, customised implant design, prosthetics and orthotics. In surgical planning, the objective of 3D printing is to provide surgical teams a visual aid (biomodels) to better plan surgical procedures. This leads to a reduction of operation time, cost, and risk. Biomodels become exceptionally helpful where there are deformities or anatomical abnormalities [91].

Development and design of devices such as guides can assist in transferring information derived from preoperative images into the operating room [93]. An example of this type of device is a bra-like guide used to transfers MRI-derived tumor localization information to breast conserving surgery (Figure 15). The bra-like plastic guide was designed to match the breast's surface [94].

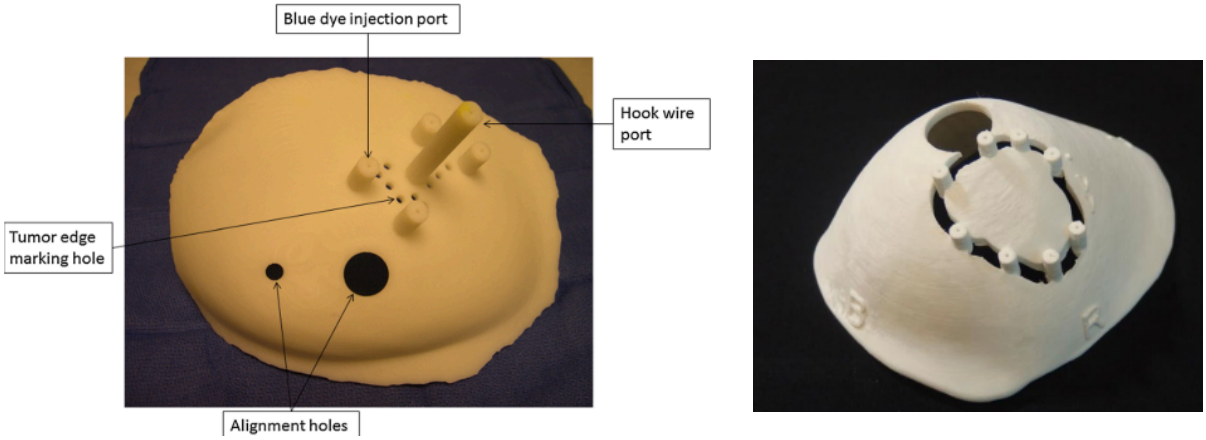

Figure 15 Surgical guide for the breast allows surgeon to mark tumour edges on the skin. Several ports enable dye to be injected. The hook wire port enables surgeon to deploy a hook wire in the tumor(Adapted from [93], [94]*)*

The fabrication of orthoses such as arm, leg, and scoliosis braces require a series of manufacturing processes such as molding and thermoforming plastic. By employing 3D printing, the manufacturing processes reduces tremendously [95] . Figure 16 and Figure 17 display orthoses created using 3D printing.

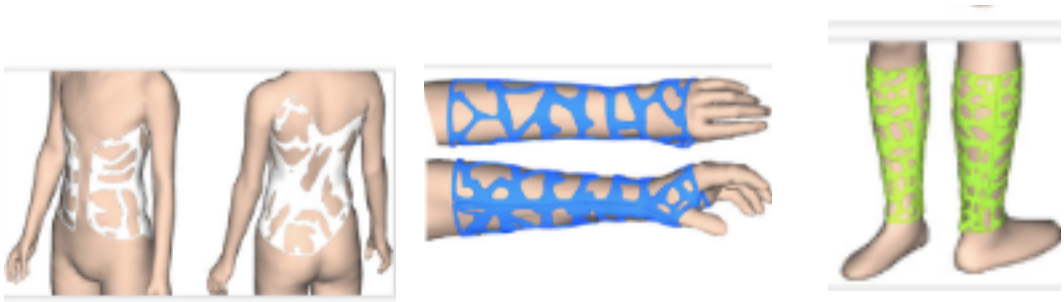

(a) (b) (c)

Figure 16 3D printed (a) scoliosis cast, (b) arm cast, (c) leg cast (Adapted from [96]

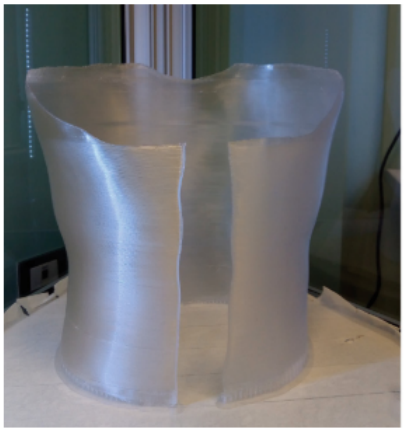

Figure 17 3D printed scoliosis brace (Reprinted from [95]*)*

2.5.2 Spine Surgery

The use of 3D printing in the field of MISS was first described in 1999 to print model of the spine entirely to assist with visualization of cases that presented complex deformity [97][98]. With the arrival of rapid prototyping, 3D printing has become a valuable adjunct for surgical specialities. As the technology advances and becomes more prevalent cost are expected to decrease while the ease of use will increase [35], [97]. Biomodels developed with the use of 3D printing have the potential to improve preoperative planning and be a valuable teaching tool [99]. 3D printed surgical guides can increase hardware placement precision and accuracy [35]. In addition, surgical guides assist surgeons to better orient patients during surgical intervention, decreasing the surgery time, costs and risks of infections [100].

Patient specific guides and templates can increase accuracy and precision of hardware placements during surgery. Potential benefits of using guides and templates include reduction of operating time and radiation exposure to patients and surgical staff [101]–[104]. Many surgical templates developed in the field of MISS are to place pedicle spine screws at the proper location [105]–[107] . Normally, pedicle screws are positioned using free-hand techniques or with the assistance of fluoroscopy. The error associated with the placement of pedicle screws using free-hand range

between 10% and 40% depending on the skill of the surgeon [105]. Surgical templates and guides for pedicle screw placements are commonly small in size that fit over the vertebra of interest. When designing such device that are used internally, the material of the surgical guide must be biocompatible and sterilized [100]. An issue that arises with the use of 3D printed pedicle guides is the potential of the guide being chipped off when drilling, posing risks to the patient [107]. Furthermore, using small and more precise instruments may preclude proper hardware fitting and placement [35].

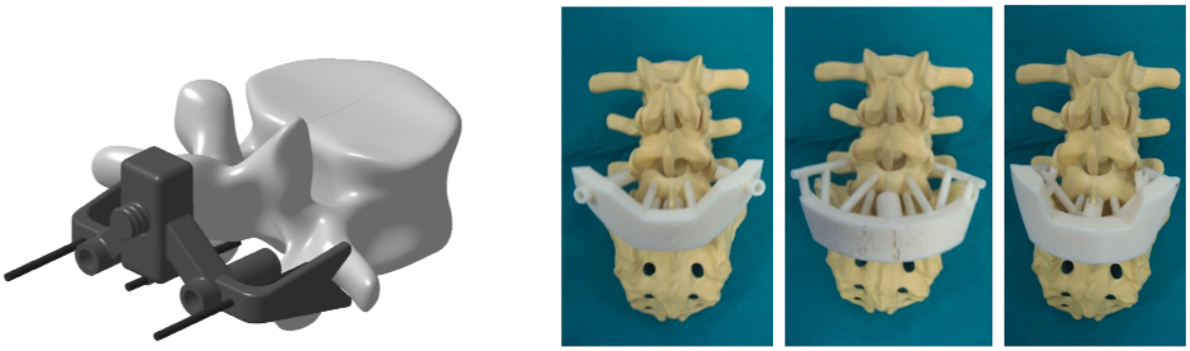

Figure 18 Template for pedicle spine screw placements(Reprinted from [105], [107]*)*

2.6 Image Registration Systems

2.6.1 Localization System

HE's Lumbar LOcation (HELLO) system was developed to assist with surgical accuracy and reduction of radiation [108]. The system consists of a self-made 9 x 18 cm radiopaque surface locator and a puncture guided device. The surface locator consists of 4 longitudinal crossbars and 19 horizontal crossbars with 1 cm intervals. For rapid recognition, a series of different patterns are made on the horizontal crossbars.

The puncture guided device is made up of three parts, a movable supporting base with 5 rollers with brakes, a micro-regulation part that can rotate freely along the arc of the vertical axis, and a 90-degree arc for trajectory guided punctures that can slide along the arc and be locked.

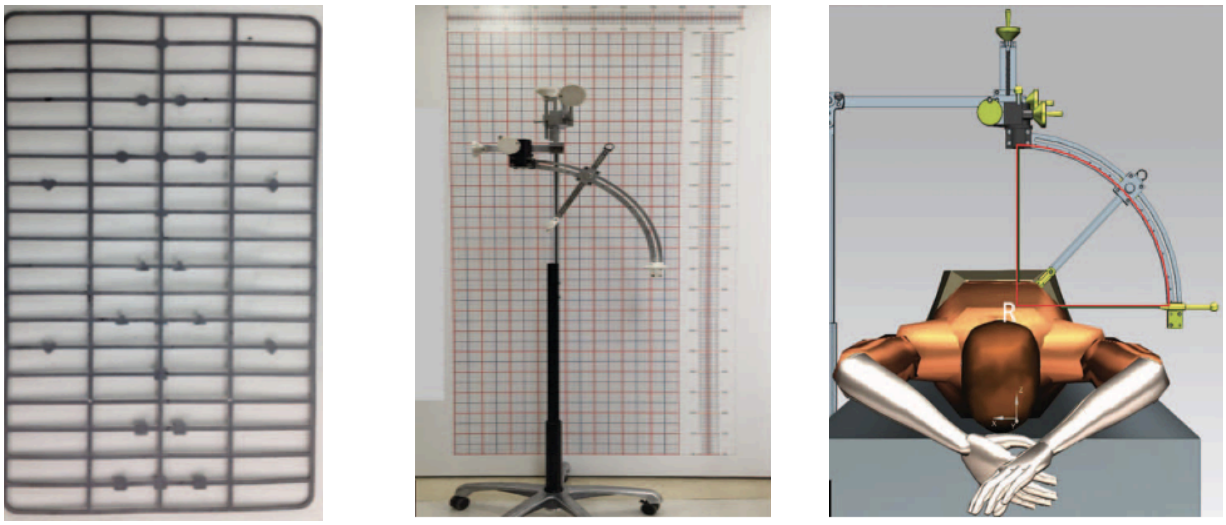

(a) (b) (c)

Figure 19 HE's Lumbar LOcation (HELLO) system: (a) surface locator, (b) puncture-guided device, (c) theory of puncture guided devises (Reprinted from [108]*)*

2.6.1.1 Surgical procedure

Two surface locators are secured in place, posteriorly and laterally, using tape. C-arm fluoroscopy is employed to obtain standard anteroposterior and lateral fluoroscopy. The target punctures are identified on the film then transferred onto the skin using the surface locators. Lastly the entry point and planned trajectory are drawn on the body. When performing MISS with the HELLO system compared to the conventional method, a 44.3% in radiation reduction was reported and a decrease in surgical time by 10.23 minutes [108].

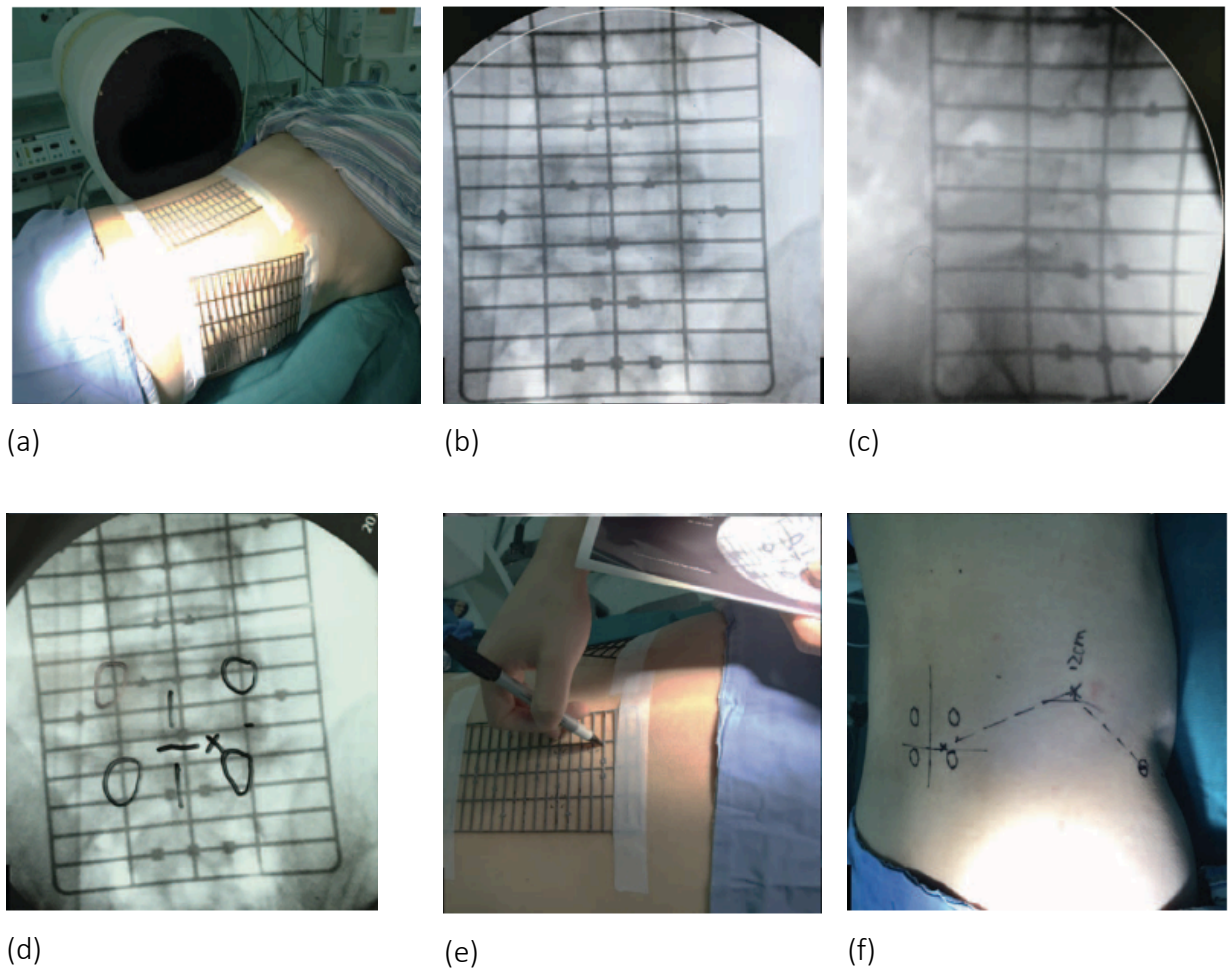

Figure 20 (a) Attachment of surface locator to skin, (b) anteroposterior fluoroscopy of surface locator, (c) lateral fluoroscopy of surface locator, (d) identification of puncture target on the film, (e) marking of puncture on the skin, (f) drawing entry point and planned trajectory (Reprinted from [108]*)*

Chapter 3: Methods

This chapter outlines the proposed workflow that generates patient specific guides to assist with spine registration during surgery (Figure 21). The data used to create the guides were obtained from MRI images. The medical images underwent preprocessing to segment the patient's skin contour. Using the skin contour points the components of the skin mesh guide were constructed. Adjustments were then made to the components to compensates for the 3D printers' restraints before carrying out the print job.

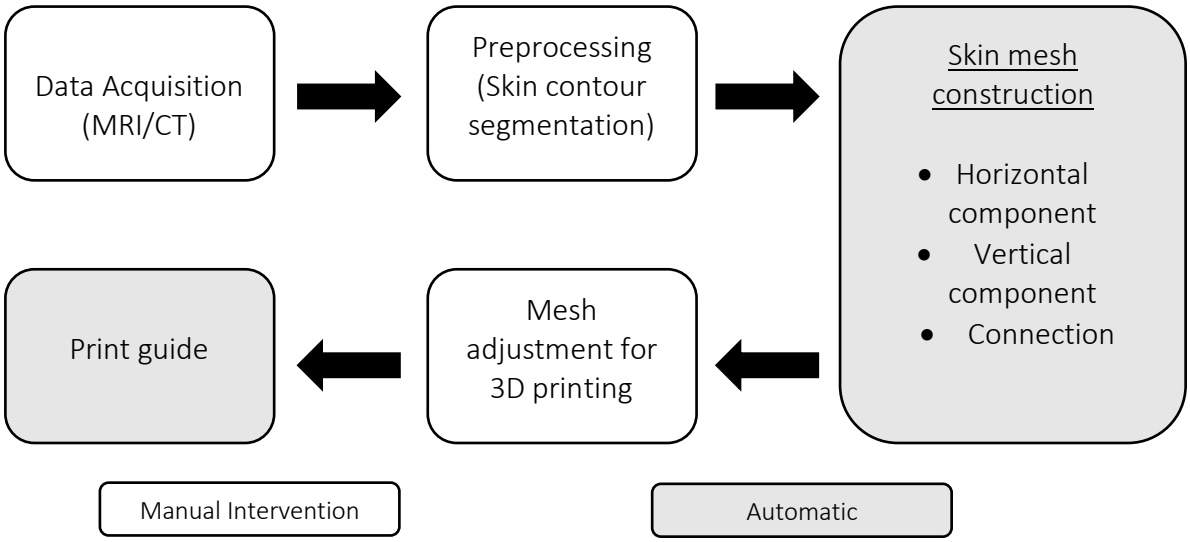

Figure 21 Workflow of patient specific guide: Data is obtained from MRI or CT images, images are preprocessed to extract contour points, using the contour points the skin mesh is constructed, adjustments are made to the surgical guide, the surgical guide is 3D printed

3.1.1 Data Acquisition

The MRI data used for this research were obtained from The Ottawa Hospital and were stored in Digital Imaging and Communications in Medicine (DICOM) format. The images contained no patient identifying information, completely anonymized. These MRI images, which were taken to examine patients abdominal, were used due to the lack of access to spine images. The dataset

contained images of three patients taken in the axial, sagittal, and coronal plane. For the purpose of this research axial images were solely used for the segmentation of the skin's contour (Figure 22).

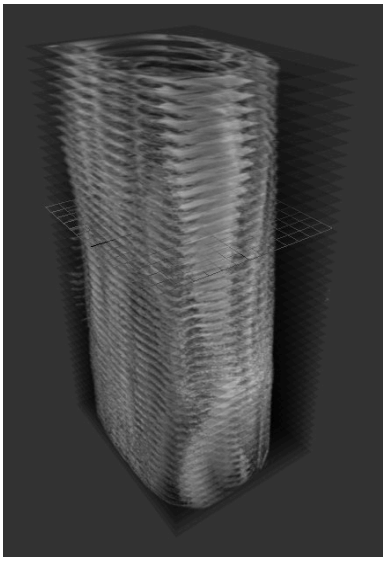

Figure 22 Compilation of a first patients' axial view MRI images

To extract the required images from the dataset, the image orientation, image position, slice thickness, echo time (TE), and repetition time (TR) tags within the DICOM files were considered (Figure 23). The tool used to accomplish this task was Python's pydicom library.

(0008, 0060) Modality	CS: 'MR'
(0008, 0061) Modalities in Study	CS: 'MR'
(0018, 0050) Slice Thickness (mm)	DS: "6"
(0018, 0080) Repetition Time (sec)	DS: "3.78"
(0018, 0081) Echo Time (sec)	DS: "1.89"
(0018, 0088) Spacing Between Slices (mm)	DS: "8.4"
(0020, 0032) Image Position (Patient)	DS:['-251.39548444748','-142.29666137695', '209.2484819293']
(0020, 0037) Image Orientation (Patient)	DS: ['1', '0', '0', '0', '0', '-1']
(0020, 1041) Slice Location (mm)	DS: "-142.29666137695"

Figure 23 Display of selected DICOM tags

The image orientation tag (0020, 0037) was examined to determine the image's plane. The tag displayed six values signifying two normalized 3D vectors. The values were direction cosines of the image plane relative to the reference coordinate system. The first three values indicate the x vector and the last three values the y vector. Table 4 shows the cosine directions and their respective viewing plane.

Table 4 Cosine direction and respective plane

Direction Cosines	Plane
['1', '0', '0', '0', '1', '0']	Axial
['0', '1', '0', '0', '0', '-1']	Sagittal
['1', '0', '0', '0', '0', '-1']	Coronal

To determine the slice location of the images, the position orientation tag was used. Selecting the lowest and highest slice level an upper and lower bound was defined. Within the set boundary, forty somewhat equally spaced images were chosen as the constructional foundation of the surgical guide. As many slice locations had multiple images, other tags including the TE and TR were examined for further inspection.

The echo time is defined as the time between the delivery of the radiofrequency impulse and the receipt of the echo signal, and the repetition time is defined as the time taken between successive pulse sequences applied to the same slice. TE and TR are both used to control the contrast of the image. Many images taken at the same slice location differed in appearance with varying regions of brightness (Figure 24). By observation, images with lower TE and TR display internal structures

more than image with greater TE and TR. Given the image position, the TE and TR were factors used to determine which image to use for further processing.

The slice thickness, which is determined by the strength of the gradient in the radiofrequency pulse and its range of frequency, was another determining factor that was considered in selecting images. The minimum standard for MRI techniques for spine imaging indicates that the slice thickness should be a maximum of 5 mm [109]. Taking all these factors into consideration the following images were selected for each patient: For patient 1 images with a TE of 109, a TR of 1200, and thickness of 6 mm were used (Figure 24), patient 2 images with a TE of 90.112, a TR of 598.964, and thickness of 6 mm were used (Figure 25) and for patient 3, images with a TE of 109, a TR of 1200, and thickness of 6 mm were used (Figure 26),.

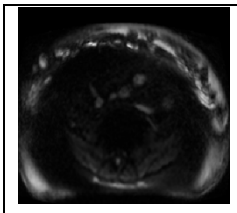	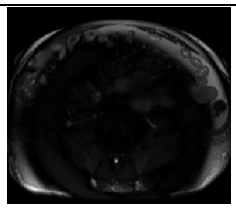	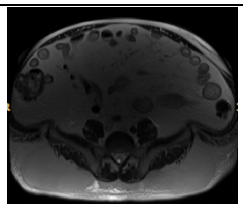	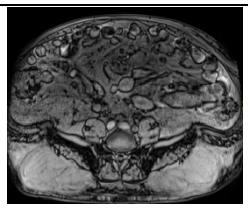	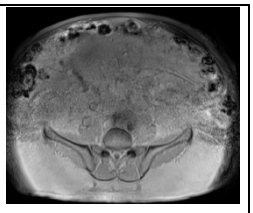
TE: 64 TR: 1600 Thickness: 6	TE: 95 TR: 1200 Thickness: 6	*TE: 109* *TR: 1200* *Thickness: 6*	TE: 2.39 TR: 6.51 Thickness: 3	TE: 4.77 TR: 6.51 Thickness: 3

Figure 24 Echo time, repetition time, and slice thickness of axial MRI image at same location for patient 1

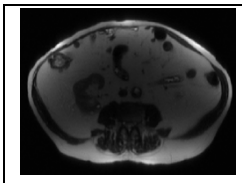	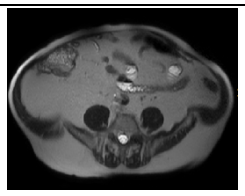	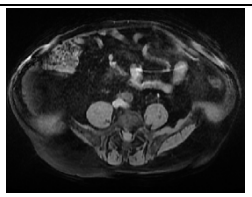	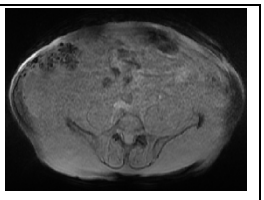
TE: 82.432 TR: 597.552 Thickness: 6	*TE: 90.112* *TR: 598.964* *Thickness: 6*	TE: 3.204 TR: 6.708 Thickness: 4	TE: 4.324 TR: 6.708 Thickness: 6

Figure 25 Echo time, repetition time, and slice thickness of axial MRI image at same location for second patient

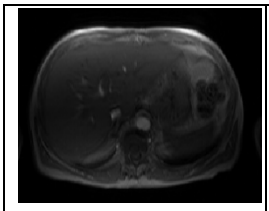	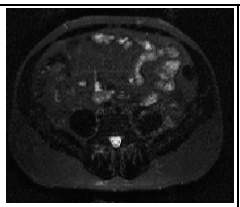	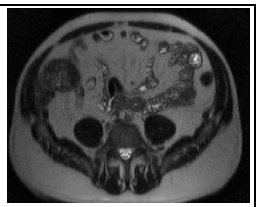		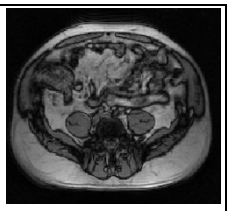
TE: 5 TR: 15 Thickness: 10	TE: 125 TR:4850 Thickness: 5	*TE: 83* *TR:1030* *Thickness: 5*	TE: 4.76 TR:174 Thickness: 8	TE: 2.38 TR:174 Thickness: 8

Figure 26 Echo time, repetition time, and slice thickness of axial MRI image at same location for third patient

3.1.2 Skin Contour Points

The contour extraction component of the workflow was completed by Jiawei Li. The contour of the patient's skin was extracted by segmenting the skin's outline from the 'air' present around the patient. Since air does not emit an MRI signal it appears black on the image. The image was first converted into pixel array in order to apply morphological transformation. Using the binary image obtained from the morphological transformation the contour points are extracted. The contour points then underwent filtering to smoothen the contour. The steps taken to extract the contour points are outlined in Figure 27 and the result of each step is displayed in Figure 28.

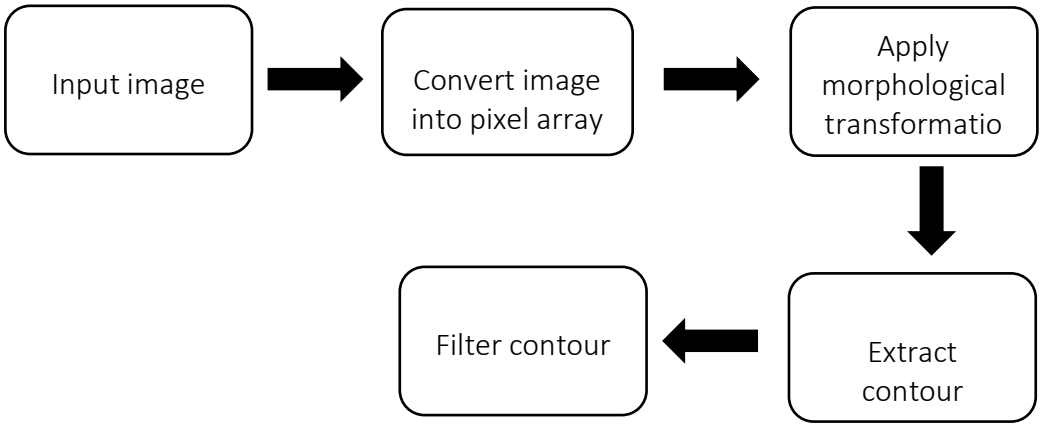

Figure 27 Steps taken to extract contour from image: 1. convert image into pixel array, 2. Apply morphological transformation, 3. Extract contour points, 4. Filter contour points

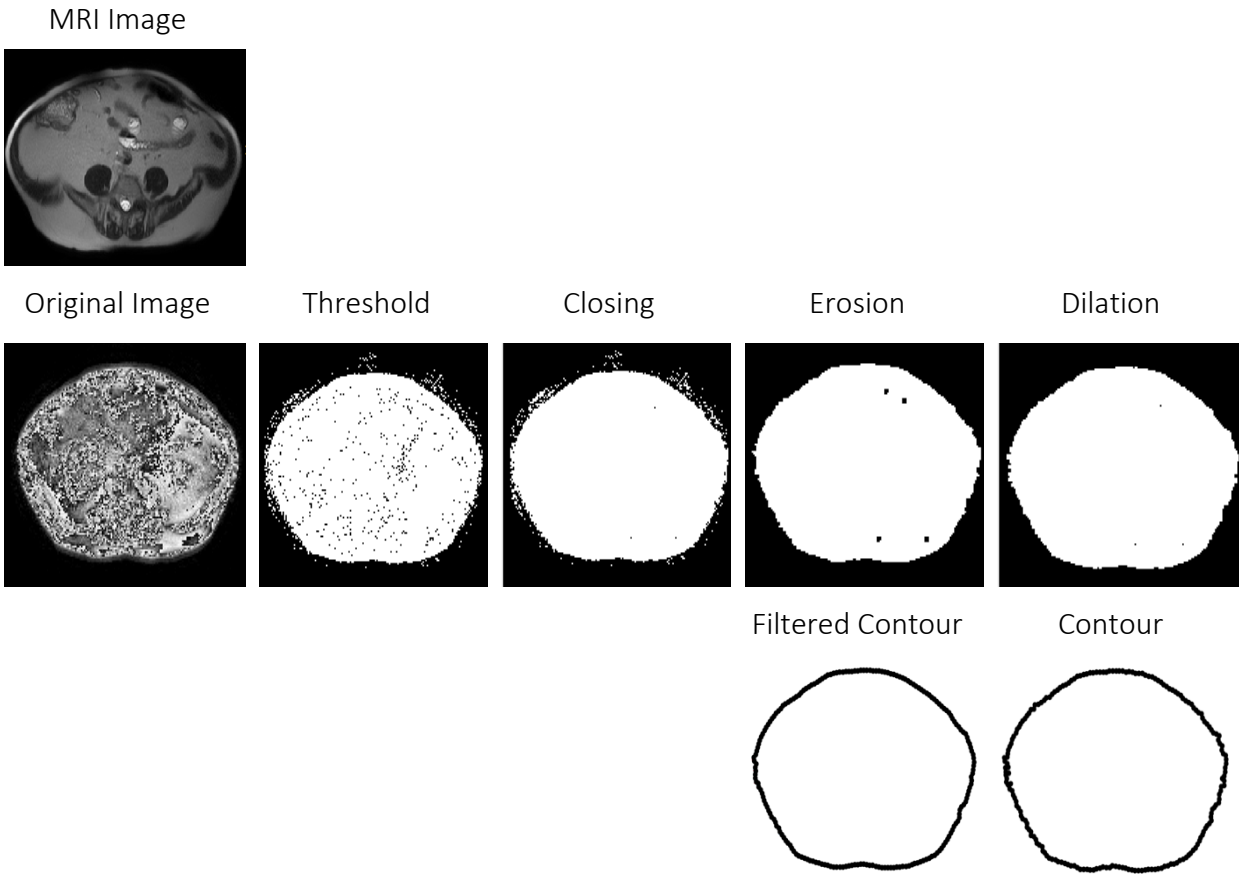

Figure 28 Steps taken to segment patient skin, 1. convert image into pixel array, 2. apply thresholding, 3. apply closing operator, 4. apply erosion operator, 5. apply dilation operator, 6. extract contour, 7. filter contour

To convert the image into an array of pixels the numpy.array function from the NumPy library was used. Once the images were in a pixel of arrays, OpenCV's cv2.threshold function was utilized, more specifically the simple THRESH_BINARY type, to obtain a binary image. A threshold value of 18 was chosen to perform thresholding to the selected images. The images then underwent morphological transformation to remove imperfections present in the binary image. The kernel used for the morphological processing was an elliptical shaped kernel of size 3. The first

morphological operator employed was closing to reduce the dark points in the foreground, followed by erosion to remove white noise around the boundary, and lastly dilation to fill in remaining gaps in the foreground. To extract the contour of the modified binary image, cv2.findContours() was used. The contour retrieval mode cv.RETR_EXTERNAL was selected to retrieve the extreme outer contour, and cv.CHAIN_APPROX_NONE was chosen for the contour approximation method to store all contour points. To approximate the polygon shape of the contour cv2.approxPolyDP function was applied next. Lastly, the np.convolve function was used to smoothen the contour curve.

3.2 Construction of Mesh Grid

The main component of the workflow was the production of the script which automatically generates the components for the surgical guide. The surgical guide was divided into components as most 3D printers' dimensions are smaller than the human's torso. Utilizing the skin contour extracted from the medical images the program was created in MATLAB for this research.

3.2.1 Horizontal Component

The horizontal components were created using the contour points as the base. Once imported into MATLAB, filtering was applied to the skin contour to obtain a smooth enclosure and have equally spaced points (Figure 29).

Using the contour points as the lower inner base layer, the upper inner, lower outer, and upper outer layers were formed. From the 40 layers obtained, obtained from the 40 selected images, between 4 and 6 were used to create the horizontal components. The lower outer layer was obtained by first calculating the distance between each contour point and the contour's center. The angle of the line joining the center point and the selected contour point was then calculated. Using the calculated angle, a thickness was added to the distance between the selected point and center to obtain the lower outer layer points (Figure 30 (a-b)). The upper inner layer was created

by adding a height value to the lower inner layer similarly a height value was added to the lower layer to obtain the upper outer layer (Figure 30 (c)).

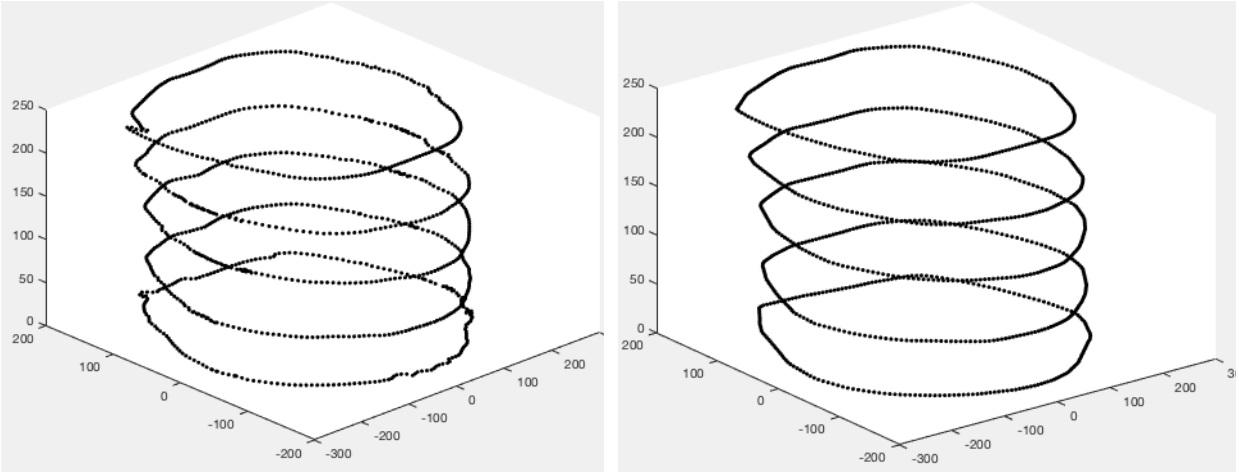

Figure 29 Imported contour points (left), filtered and equally spaced contour points (right)

A gap, of a chosen size, between the two adjacent points define the thickness of the vertical components. Joints that would connect the vertical and horizontal components together, were created where gaps were left in the horizonal components (Figure 31(a)). The mesh for the horizontal components were created using the regions between two gaps. To create the meshes MATLAB's triangulation function was used which required two inputs, vertices and faces. The horizontal component mesh was divided into four sections, top, bottom, front, and back. The vertices used to create the top mesh were the upper inner and outer points and the faces were formed using the two adjacent points on each layer. For the bottom mesh the lower inner and outer points were used, the front mesh utilized the lower outer and upper outer points, and lastly for the back mesh the lower inner and upper inner points were used (Figure 31(b)).

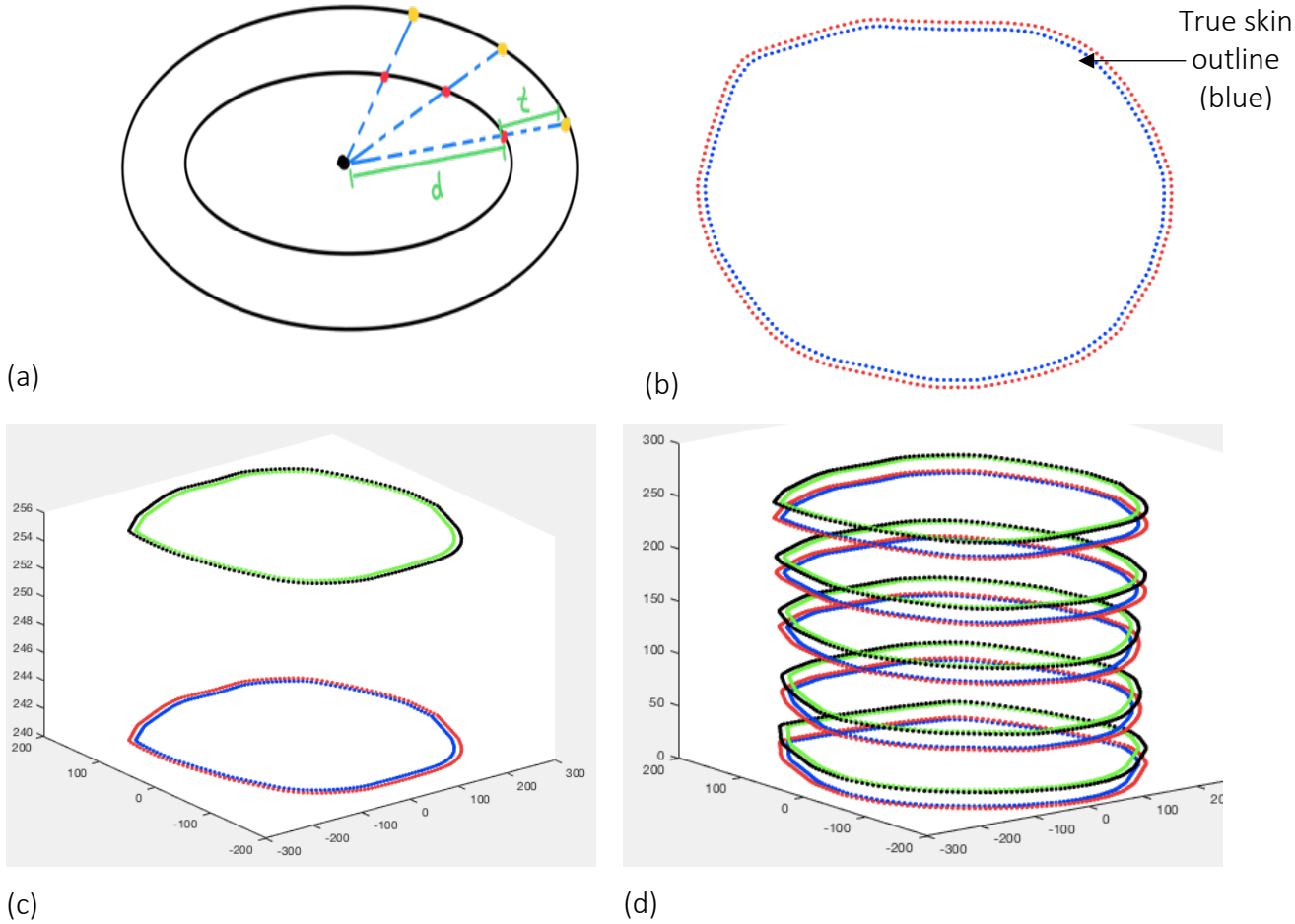

Figure 30 (a) Thickness (t), was added to the distance (d) between the centre and contour point (b) Lower inner layer (blue) and the lower outer layer is in (red),where the lower inner layer coincides with the patients skin (c) Upper inner layer is green and the upper outer layer is in black, (d) All layers together

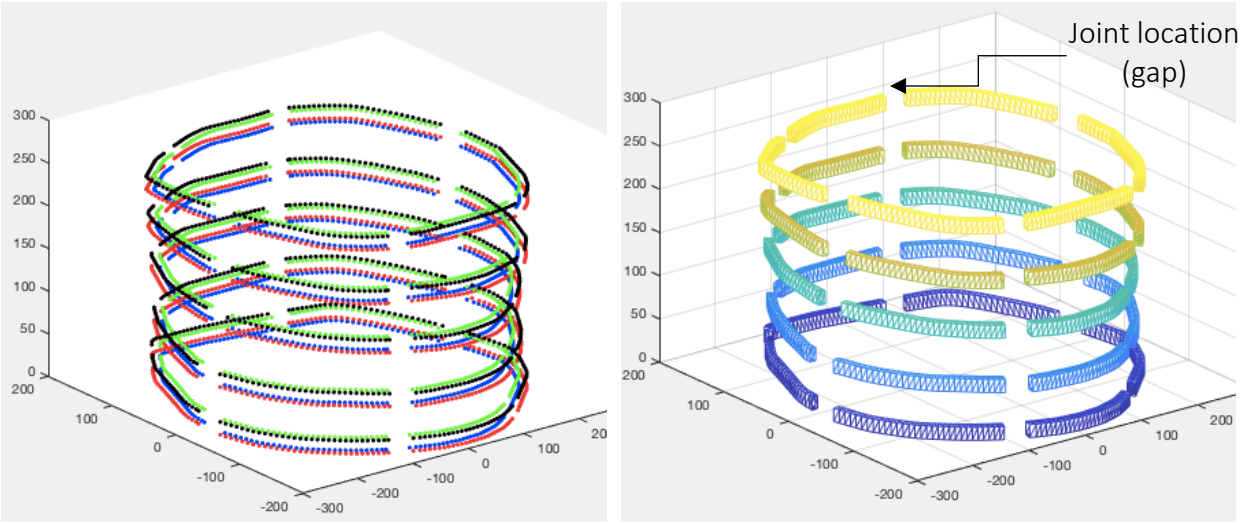

(a) (b)

Figure 31 (a) Points used to create horizontal mesh components, (b) Horizontal mesh where the gaps indicate the thickness of the vertical

3.2.2 Vertical Component

N number of points were selected from the upper most horizontal layer as the location of the vertical component. The thickness of the vertical component was determined by the thickness of the horizontal component which can be changed to ensure for stability (Figure 32(a-b)). More specifically the vertical thickness equates to half of the horizontal's thickness. The width of the vertical component, a parameter that can also be modified, was obtained by selecting adjacent points to the points chosen for the vertical component's location.

Similar to the horizontal components, the triangulation function in MATLAB was employed to create the mesh for the vertical components and the mesh was divided into the 4 parts, top, bottom, right side, and left side (Figure 32(c)). The gaps left in the horizontal and vertical components are the locations of the joints connecting and securing the two components together.

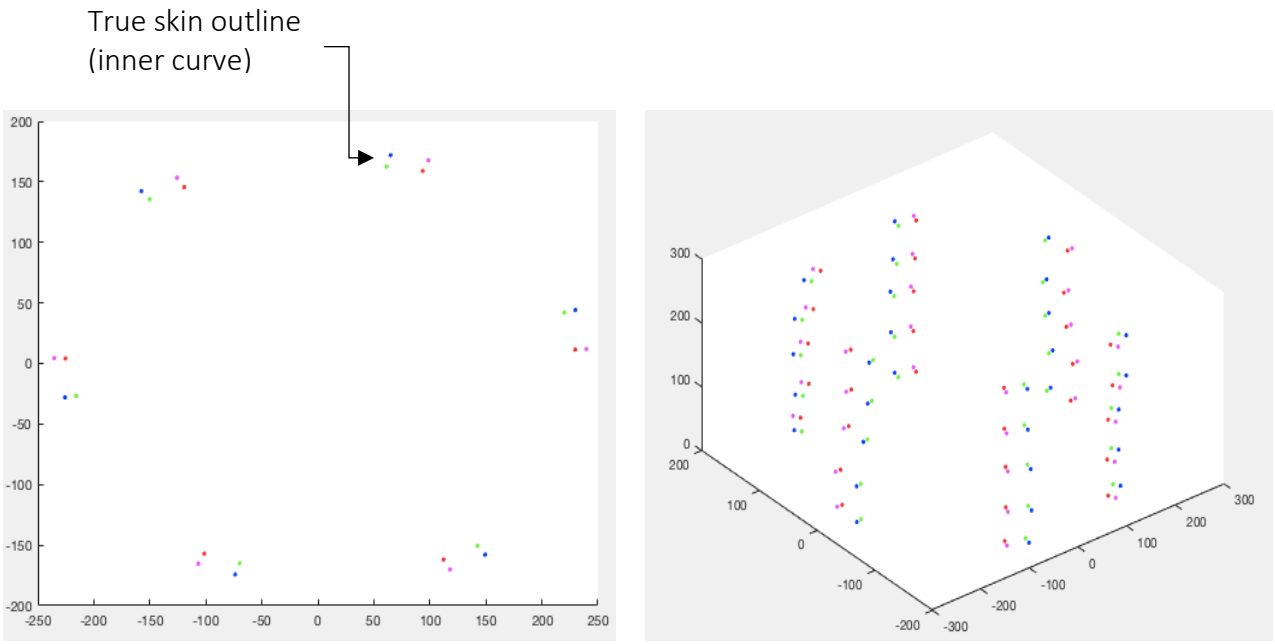

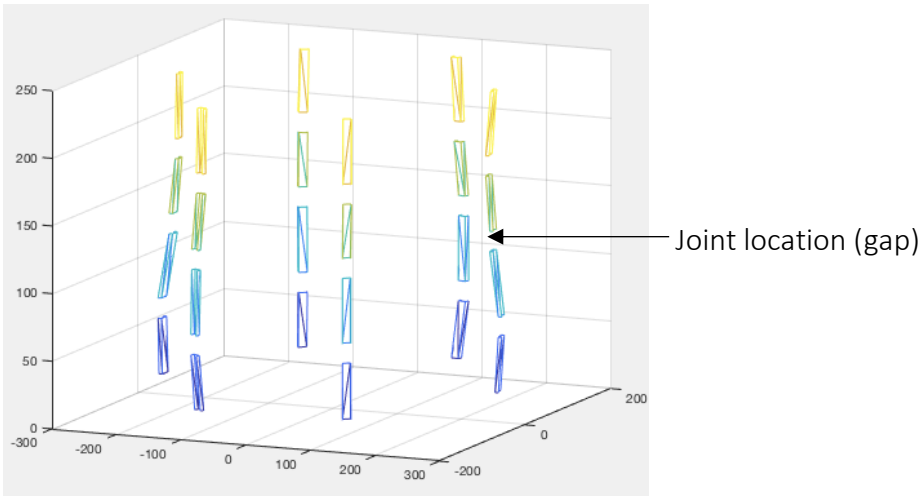

Figure 32 (a) Location and thickness of vertical components, (b) Points used to create mesh for vertical components, (c) Vertical component mesh

3.2.3 Connecting Components

A simple technique used to connect 3D printed parts together is by applying cyanoacrylate, also known as superglue. While superglue dries quickly, repositioning parts becomes really difficult once applied. For materials such as Polylactic acid (PLA), acrylonitrile butadiene styrene (ABS), and polyethylene terephthalate (PETG) super glue is an adequate option for joining parts, however, for material such as thermoplastic elastomer (TPE), thermoplastic polyurethane (TPU), nylon, and other flexible material it is not. To ensure parts can be attached together independent of the choice of material joints were added to the horizontal and vertical components. By implementing joints into the design of the guide, components can be assembled and disassembled without the usage of any adhesives.

The main criteria for selecting the choice of joinery were resistant against pulling and ease of manufacturing. The dovetail joint, widely used in conventional woodwork, met these requirements [110]. The design of the dovetail joint resists bending moments and tractions restricting movements to one degree of freedom [111]. The dovetail joint consists of a pin (intruded) and tail (extruded). In the design of the surgical guide, the pins of the dovetail joint were located on the horizontal components (Figure 33). while the tails were located on the vertical components (Figure 33 (b)).

(a) (b)

Figure 33 (a) Pin of the dovetail joint, (b) tail of the joint (right)

The dovetail joint was created using the midpoint between in the inner and outer layers of the horizontal layer. Using the midpoints, lower inner and outer, and upper inner and outer points the meshes for the joints were created (Figure 34 and Figure 35).

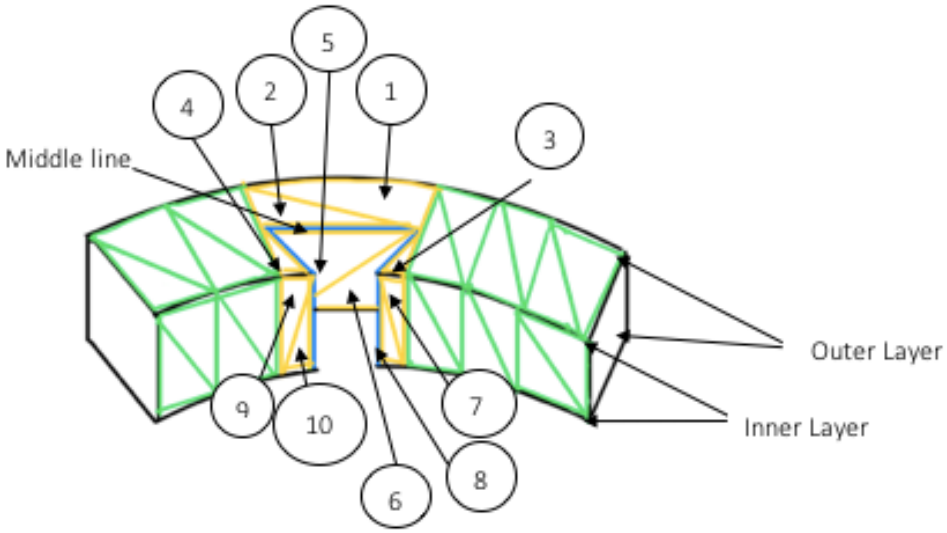

Figure 34 Section of horizontal component. Visible meshes are numerated and heighted in yellow.

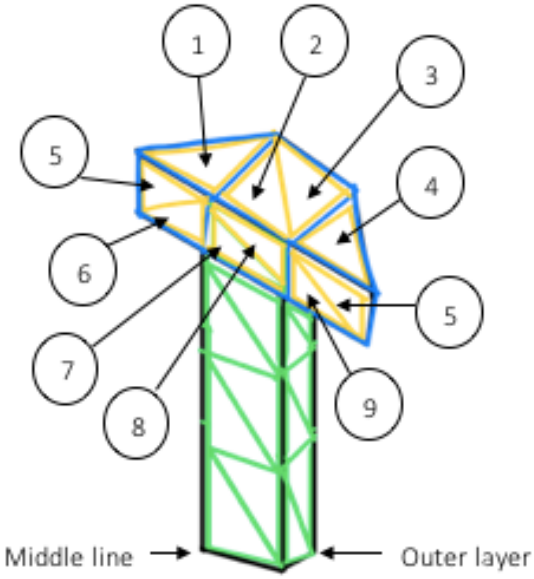

Figure 35 Section of vertical component. Visible meshes are numerated and heighted in yellow.

3.3 Component Adjustments and Assembly

Before proceeding to printing, a few adjustments were necessary to be made as a result of the printer's size limitation. The UltiMaker 2+ (Figure 36), which utilizes FDM technique, was the 3D printer used to produce the surgical guide prototype. The accuracy of the printer varies between -163μm and 12μm depending on the shape being printed [112]. The maximum print dimension that the UltiMaker 2+ can accommodate is 223 x 223 x 205 mm which is smaller than an average adults' torso. Consequently, the surgical guide components were divided into subparts to ensure the print dimension did not exceed the printer's size limit (Figure 37).

Figure 36 Ultimaker 2+ 3D printer used to produce the surgical guide prototype

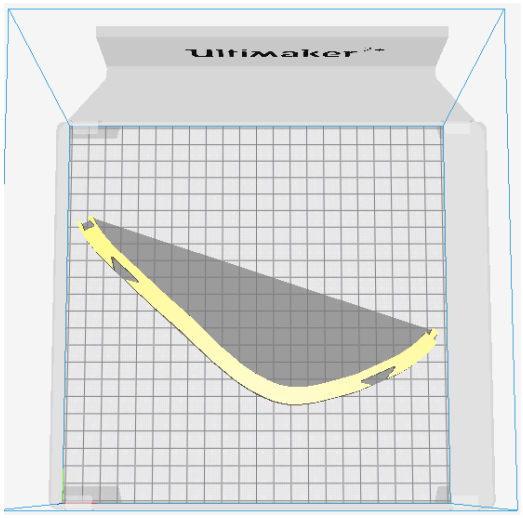

Figure 37 A subsection of the horizontal component in Cura (slicing software)

The horizontal components were divided into 4 subsections and the vertical components into 2 subsections. For the application of MISS, the ventral portion of the horizontal components was removed to avoid any discomfort it may cause patients when they lie in prone position on the surgical table (Figure 38).

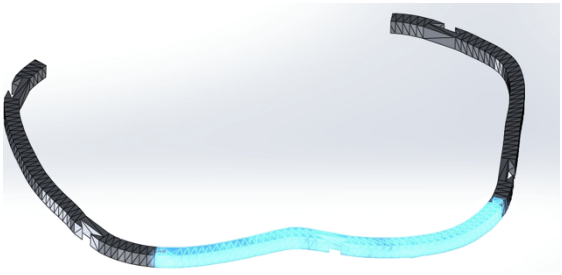

Figure 38 Ventral portion is removed from the horizontal component and the layer is divided into three section to fit the 3D printer's bed

In addition to the division of components, in order to reduce the stress associated with the connection of two parts, fillets were added to the tails and pins of the dovetail joints. To account

for the joinery tolerance, a clearance of 0.4 mm was also added to pins of the dovetail. A value of 0.4mm was chosen for the material and printer used. The choice of material and printer may yield a different value. A computer-aided design (CAD) software was employed to perform these modifications. For this research SolidWorks was used. The STL file provided by MATLAB was imported into SolidWorks as a solid part then exported as a STL file for printing.

3.3.1 Assembly

The guide requires assembly of the components before placing the it on the patient. As the components are printed markings are made to differentiate each component and allow for rapid assembly. Similar to a back brace used for scoliosis the guide was created from the back of an individual thus it matches the curvature of the individual's back. This allows for the physician to identify where to place the guide.

3.4 3D Printer Setup

Each part was printed by first converting the STL file into G-code using the chosen 3D printer's slicing software. Cura was the slicing software used in this research. As the performance and output quality of each printer differs, the print setup may require some tuning. The nozzle on the Ulitmaker 2+ varies from 0.25 mm to 0.8mm. To reduce print time the 0.8 nozzle was used. Apart from infill percent and generate support, interface elements were left to default. An infill of 10% was chosen which provided structure stability and ease of support material removal. PLA was the material used as it was readily available. Support material was added to the vertical components as some overhang was present.

Chapter 4: Result

As displayed in Figure 39, the script created was able to automatically generate digital models of the horizontal and vertical components of the surgical guide for each of the three patients. The script allows users to adjust parameters such as the number and placements of the vertical components (Figure 40), the thickness of the vertical components (Figure 41), and the removal/addition of certain horizontal components (Figure 42).

	Horizontal Component	Vertical Component
Patient 1	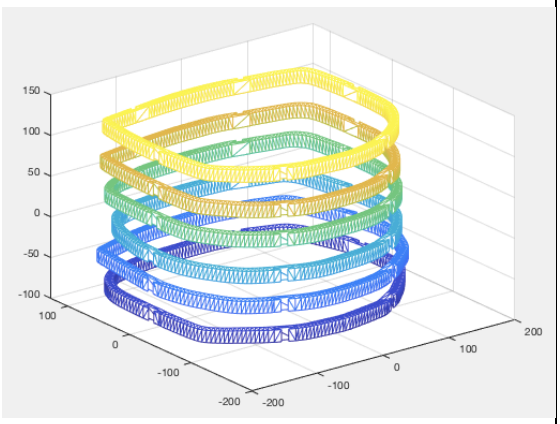	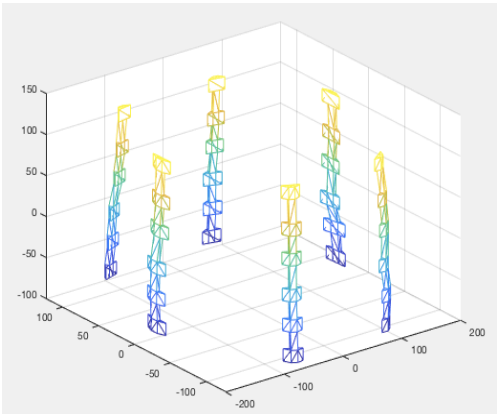
Patient 2	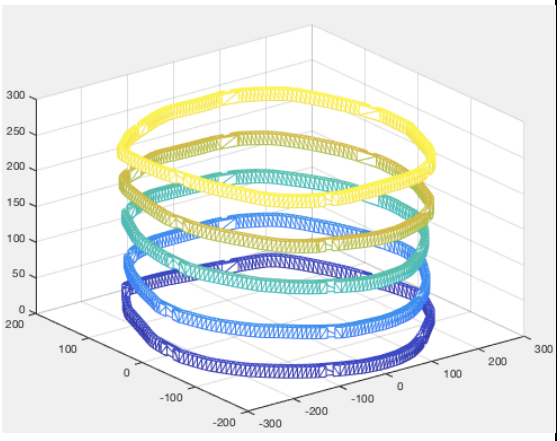	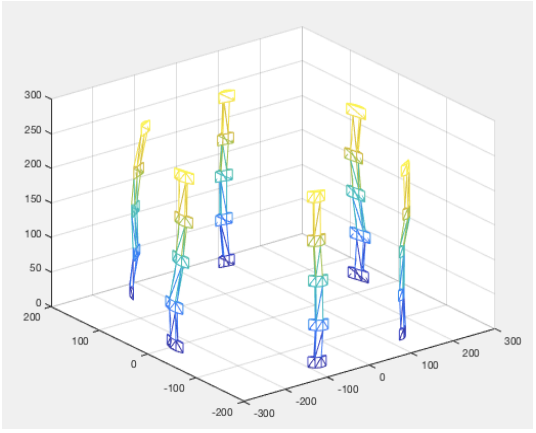

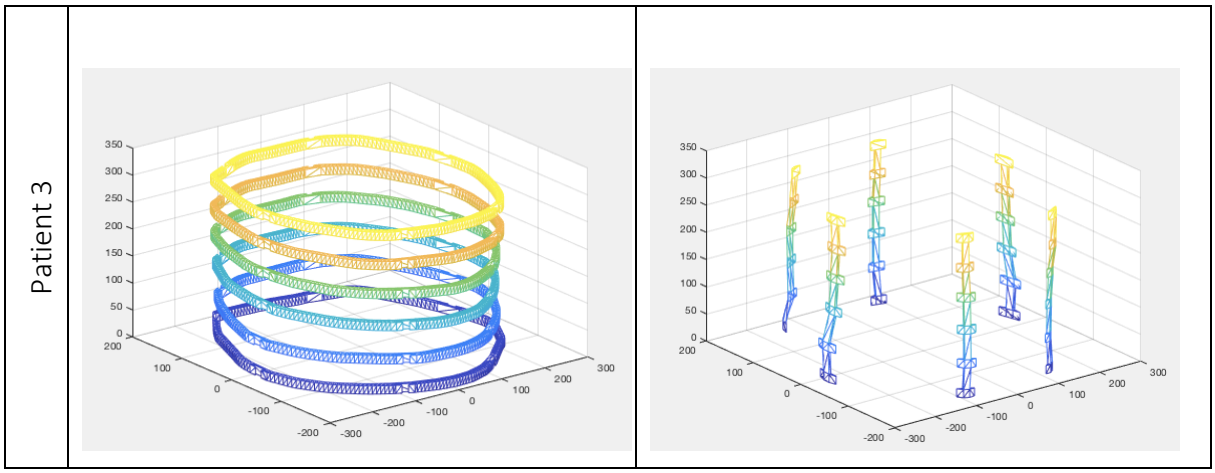

Figure 39 Horizontal and vertical components for three patients

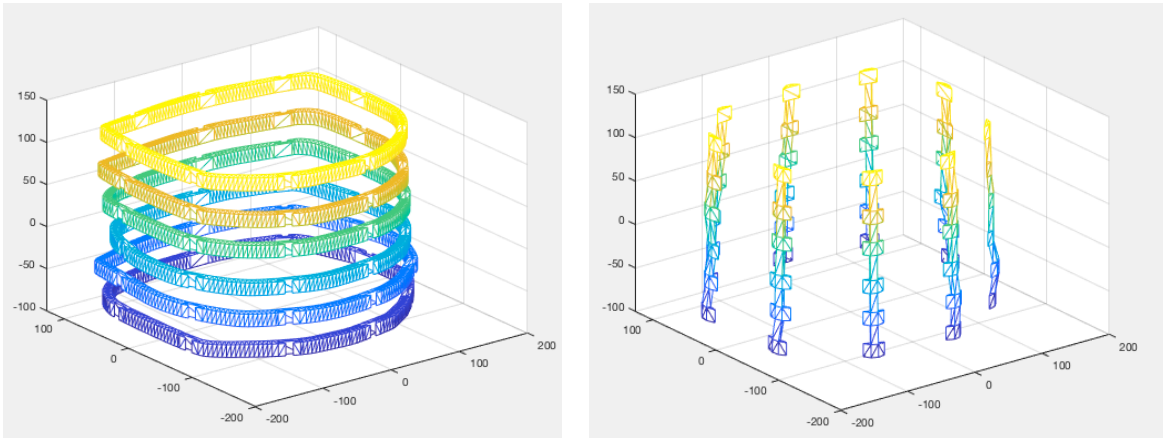

Figure 40 Increase number of vertical components from 6 to 9 (patient 1)

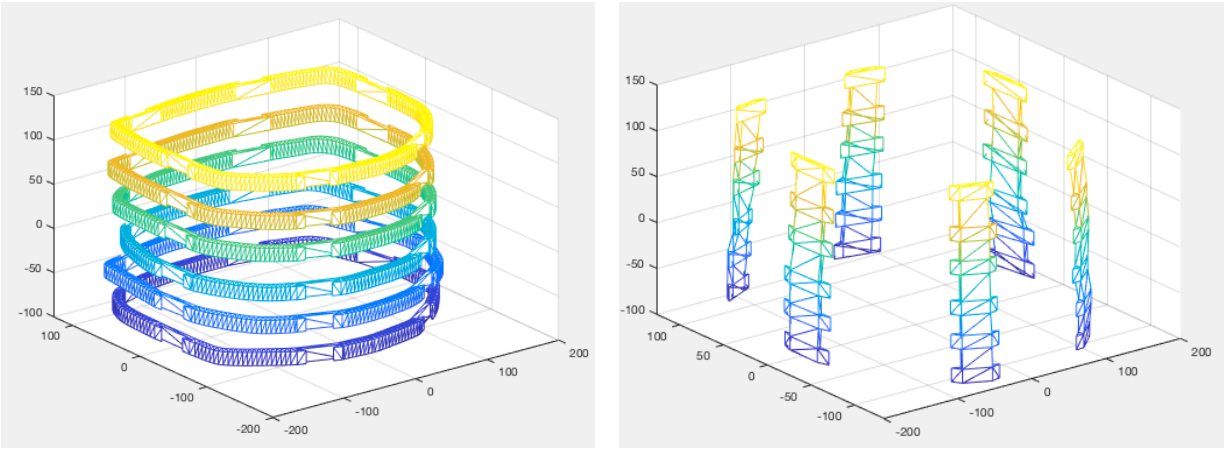

Figure 41 Double the thickness of the vertical component (patient 1)

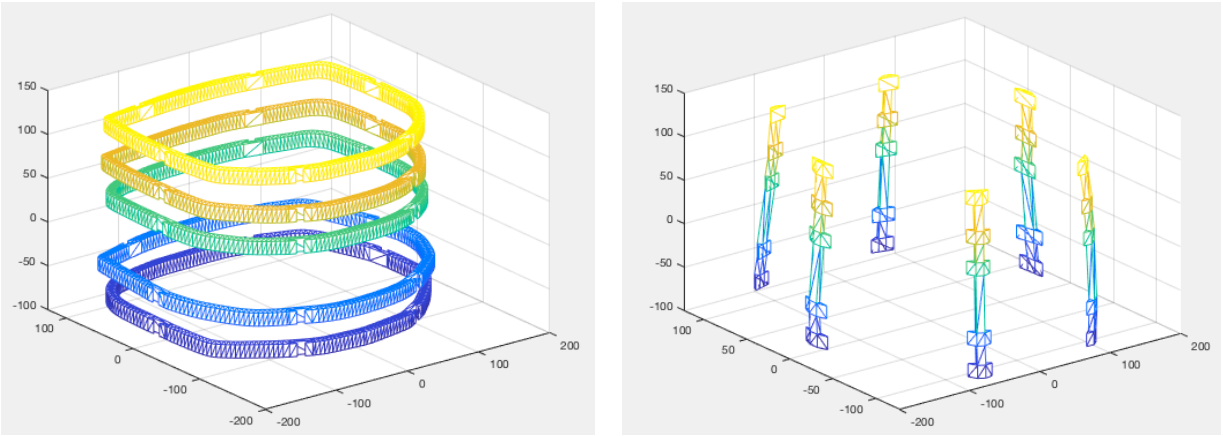

Figure 42 Removal of fourth horizontal component (patient 1)

Chapter 5: Validation

To validate the script's ability to produce a 3D printed surgical guide that would fit over a patient's back, a guide was produced for a mannequin. The mannequin was 192 cm tall and had a 30 cm torso (Figure 43). Due to the lack of access to an MRI, the skin contours of the mannequin were extracted from data obtained from a 3D scanner. The 3D scanner used was Creaform Go! Scan 3D which has an accuracy of up to 0.1mm (Figure 44) [113]. The mannequin was scanned from neck to thigh taking approximately 25 minutes producing a STL of the mannequin.

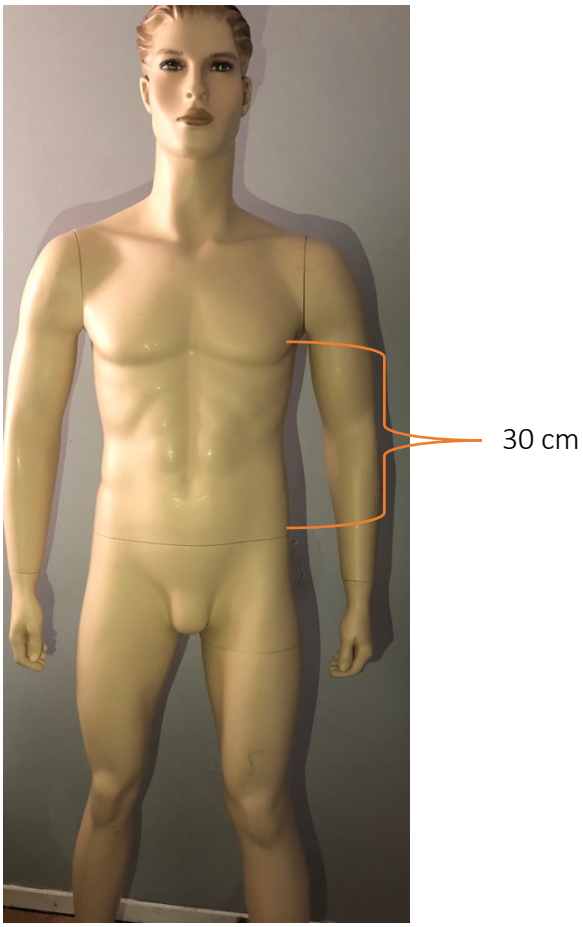

Figure 43 Adult mannequin used for validation

Figure 44 Creaform three-dimensional scanner

A MATLAB script was written to extract the contour from the SLT file. Using MATLAB, the regions between the nipple line and hip were isolated. A plane at a chosen height within the region was set to intersect the mesh. The cross-section of the mesh at the plane location resulted in the outer contour of the mannequin (Figure 45). The centre of mass of each layer was not (0,0,z), where z was the height of the layer, therefore, the centre was shifted before importing contours into the MATLAB script that automatically generates the surgical guide components.

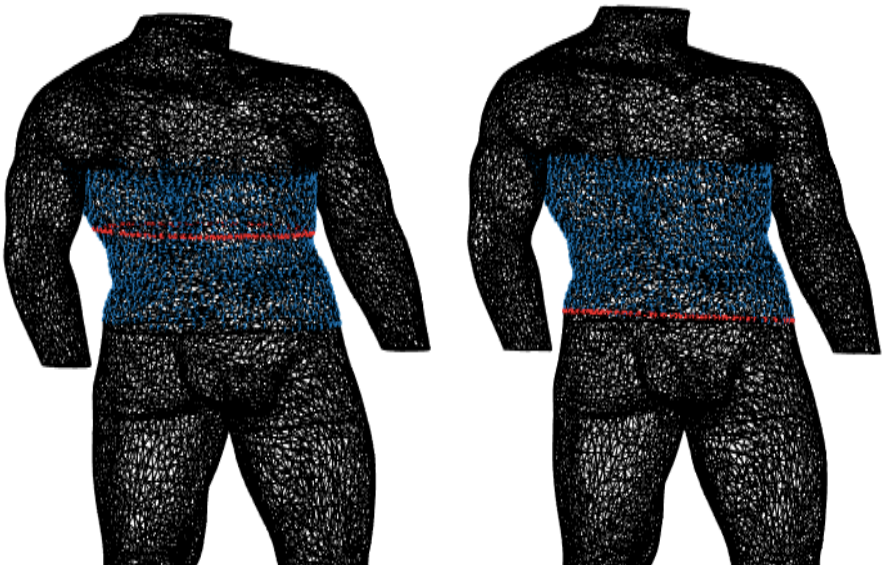

Figure 45 Mannequin mesh shown in black. Region between the nipple line and hip is highlighted in blue. The resulting contour of the plane intersecting the mesh at a given height is displayed in red (two levels shown)

Figure 46 displays the horizontal components with its associated vertical components for the mannequin. The number of contours layers importer were 10 and 6 vertical components were selected.

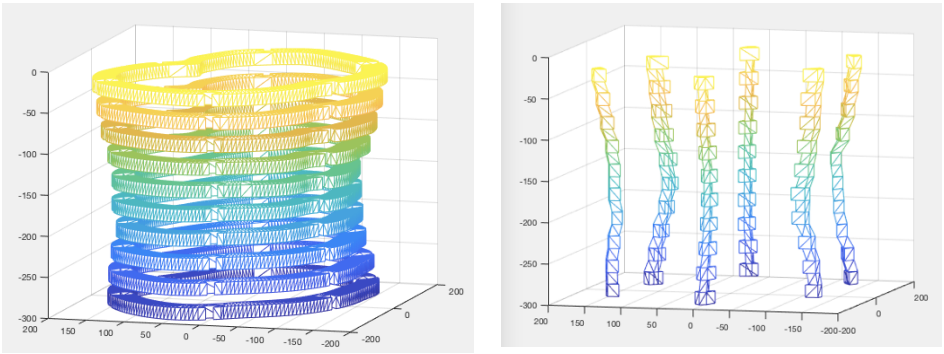

Figure 46 Horizontal component with associated vertical component of the mannequin

5.1 Prototype

Using the horizontal and vertical components generated from the script, adjustments were made using the CAD software SolidWorks to yield the digital surgical guide shown in Figure 47.

Figure 47 CAD model of surgical guide for the mannequin

Figure 48 displays the printed and numerated horizontal and vertical components before assembly. The assembled surgical guide is displayed in Figure 49 and Figure 50. The maximum gap between the horizontal components and the mannequin was 0.8 cm and the maximum gap between the vertical components was 1.5 cm. The total amount of material used to create the protype was approximately 300 grams taking around 12 hours to print. The main source of error contributing to the gap between the horizontal components and patient was due to the position of the mannequin's arms being placed by the side as opposed to over the head when it was being 3D scanning.

Figure 48 Printed horizontal and vertical components before assembly

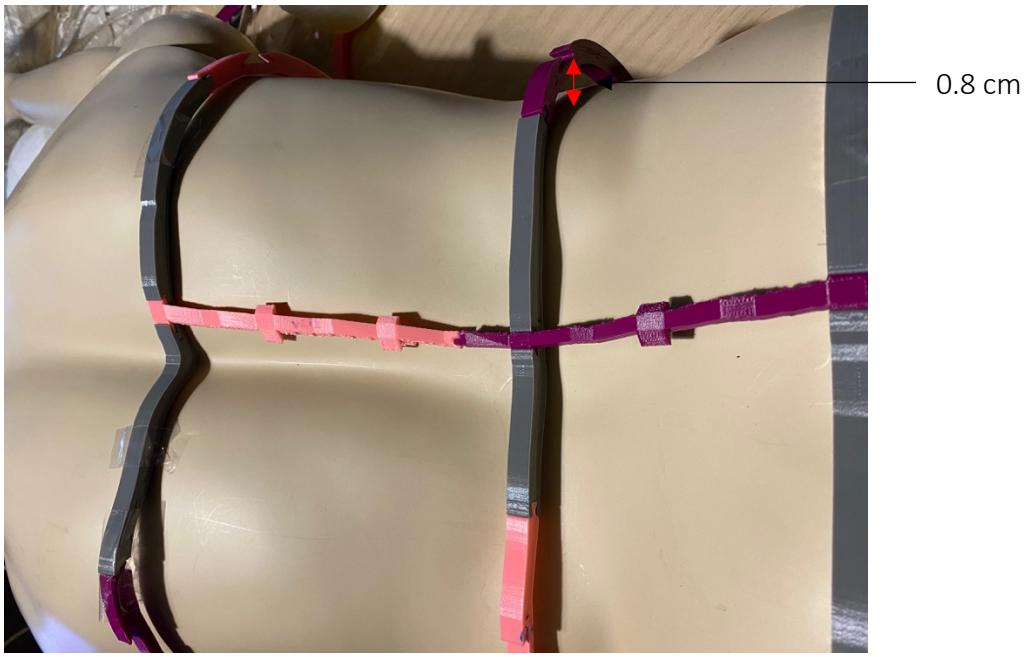

Figure 49 Top view of prototype of mannequin

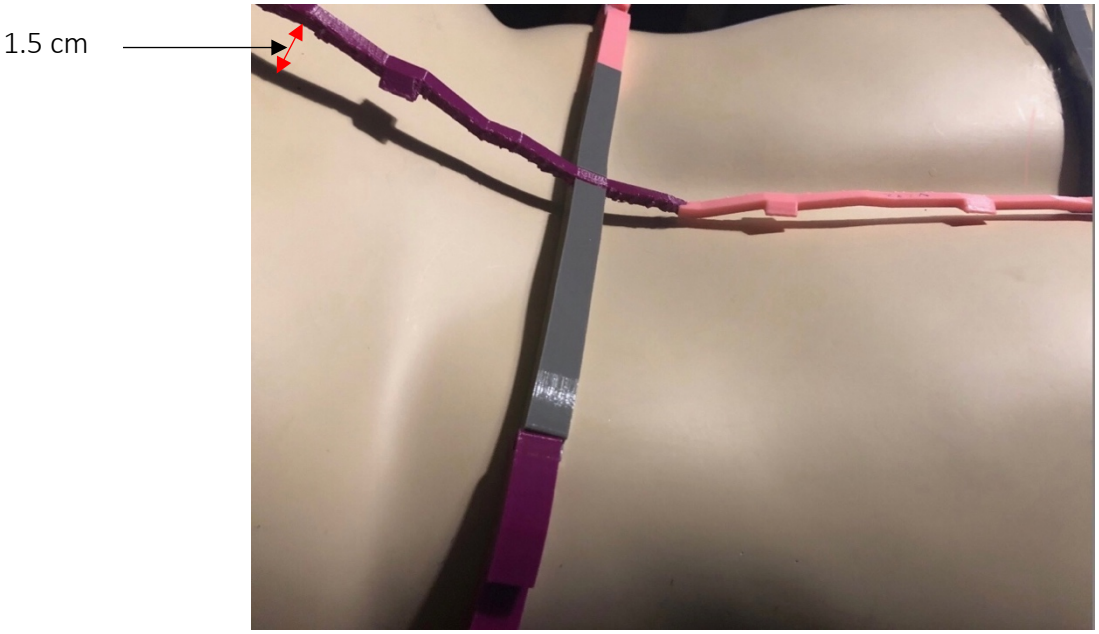

Figure 50 Side view of protype on mannequin

Chapter 6: Discussion

The script component of the proposed workflow was able to automatically generate the digital horizontal and vertical components for three patients. The created script allows physicians to adjust parameters such as component thickness, joint size, and the number of vertical and horizontal components in order to achieve optimal design while maintaining structural stability. While the script automatically produces the digital horizontal and vertical components, manual intervention is needed to produce the physical surgical guide. These interventions include removing the anterior aspect of the surgical guide, dividing components into printable sizes, and adding fillets and clearance at joint locations.

The workflow was validated through the use of a mannequin due to the lack of access to patients. The protype created for the mannequin fitted over the mannequin's back with an average vertical gap of 1.1 cm and a maximum vertical gap of 1.5 cm. The average gap for the horizontal component was 0.4 cm with a maximum horizontal gap of 0.8 cm. The averages were obtained by taking four measurements between joints using a ruler and a measuring tape. Taking into consideration the equipment used, a gap of 0.5 cm $\pm$ 3mm was deemed to be acceptable for the horizontal component.

As the mannequin was scanned with its arms down, it can be considered as the main reason for the maximum horizontal gap being located on the lateral aspects of the torso. By 3D scanning the mannequin with its arms above its head, a reduced gap can be expected. Also, as the components were divided into sections, the error associated with the assembly of the part could be a source of error. Other contributing factors creating gaps along the horizontal component include the error associated with the handling of the 3D scanner and printer, the errors associated with the devices themselves, and the segmentations of the components. A snug fit of the guide against the

patient would be desirable, however, a uniform gap of 2mm can provide room for padding placement, for comfort and preventing slipping of the components.

The gap between the vertical component and the mannequin will always be present as the joints were created using half the horizontal components' thickness. As the vertical component does not follow the contour of the body, contrary to the horizontal components, the gaps were expected to be larger. The purpose for the vertical components was to keep the horizontal components in place while keeping the gap between the horizontal components and the mannequin to a minimum. By designing the guide as a wireframe, instead of a solid guide with gaps at points of interests, the overall print time and material usage are reduced.

The proposed workflow has the potential of providing an affordable alternative to existing technologies such as navigation system to assist with MISS. Systems such as the HELLO system and navigation system require re-registration if the position of the patient shifts, thus increasing the exposure to radiation. Furthermore, navigation systems along with the imaging technology of choice and surgical tools can cost well over a million dollars. More research is required on cost effectiveness to financially justify the purchase of navigation systems [114].

The HELLO system provides a cost-effective solution while using systems available in operating rooms. The proposed surgical guide can be seen as an improvement to the HELLO system. Instead of using multiple standard sized surface locators, which are held in place with tape, the proposed system generates a single customized guide. While the trajectory of the incisions is determined during surgery for the HELLO system, the proposed system allows surgeons to preoperatively plan the trajectory of tools. The proposed surgical guide can also potentially assist with reducing the learning curve associated with MISS as the patient's intraoperative body position matches their preoperative position.

6.1 Limitations

The main limitation of this research was the lack of access to patients, an assortment of printing material, and imaging technology. An element captured with the MRI and not the 3D scanner, was the deformation of the skin. When a patient undergoes an MRI, they remain laying for a period of time resulting in some deformation of the body. Also, a 3D scanner does not contain information that can be used to construct a biomodel. Testing various 3D printing material would allow for the selection of more suitable material for the surgical guide. A limitation inherent to 3D printing that was encountered in the process of constructing the surgical guide was surface roughness. This issue could be addressed by implementing soluble materials as supports. The limitation associated with this foundational work were primarily challenges to gain access to various 3D printers and material as well as access to patients. The 3D printers employed during this research are typically used for creating prototypes and not tools used in the operating room.

Chapter 7: Conclusion and Future Work

The purpose of this research was to develop a foundational workflow that generates patient specific surgical guide to assist with image registration during MISS. By importing the contour of patient's skin obtained from preoperative MRI images a script that automatically generates the components of the surgical guide was created. With the assistant of CAD software modification were made to the components to comply to the selected 3D printer's limitations. To validate the workflows ability to generate surgical guides that fit over patient's posterior, a guide was created for a mannequin. Due to the lack of access to MRI a 3D scanner was used to obtain the data required to extract the mannequin's contour. The maximum gap between the mannequin and the guide was 0.8 cm for the horizontal components and 1.5 cm for the vertical components.

The proposed next steps in this research includes producing surgical guides for patient, consulting with healthcare professionals , calculating trajectory of tools, adding tool supports onto the guide, and testing various materials and 3D printers for optimal design. In addition, by proposing a protocol for image acquisition, registration can be done efficiently as the patient will be orientated in the same manner during image acquisition and surgery. Consultations with healthcare providers will help determine whether the patients' intraoperative and preoperative positions are aligned with the help of the surgical guide. Additionally, any issues that may arise due to the deformability of the torso can be addressed during consultation. Also, adding straps and padding to the guide will secure the device onto the patient restricting movement.

Chapter 8: Reference:

[1] A. G. Gallagher and C. D. Smith, “From the operating room of the present to the operating room of the future. Human-factors lessons learned from the minimally invasive surgery revolution,” *Semin. Laparosc. Surg.*, vol. 10, no. 3, pp. 127–139, 2003.

[2] P. D. Patel, J. A. Canseco, N. Houlihan, A. Gabay, G. Grasso, and A. R. Vaccaro, “Overview of Minimally Invasive Spine Surgery,” *World Neurosurgery*, vol. 142. Elsevier Inc., pp. 43–56, 2020.

[3] G. B. Brodano *et al.*, “Transforaminal lumbar interbody fusion in degenerative disk disease and spondylolisthesis grade I: Minimally invasive versus open surgery,” *J. Spinal Disord. Tech.*, vol. 28, no. 10, pp. E559–E564, 2015.

[4] Y. Kawaguchi, H. Matsui, and H. Tsuji, “Back muscle injury after posterior lumbar spine surgery: Part 2: Histologic and histochemical analyses in humans,” *Spine*, vol. 19, no. 22. pp. 2598–2602, 1994.

[5] R. Gejo, H. Matsui, Y. Kawaguchi, H. Ishihara, and H. Tsuji, “Serial changes in trunk muscle performance after posterior lumbar surgery,” *Spine (Phila. Pa. 1976).*, vol. 24, no. 10, pp. 1023–1028, May 1999.

[6] Y. Kawaguchi, H. Matsui, and H. Tsuji, “Back muscle injury after posterior lumbar spine surgery: A histologic and enzymatic analysis,” in *Spine*, 1996, vol. 21, no. 8, pp. 941–944.

[7] Y. Kawaguchi, H. Matsui, and H. Tsuji, “Back muscle injury after posterior lumbar spine surgery: Part 1: Histologic and histochemical analyses in rats,” *Spine (Phila. Pa. 1976).*, vol. 19, no. 22, pp. 2590–2597, 1994.

[8] H. H. Mathews and B. E. Mathern, “Percutaneous procedures in the lumbar spine,” *Princ. Tech. Spinal Surg.*, pp. 731–745, 1998.

[9] J. D. Schwender, L. T. Holly, D. P. Rouben, and K. T. Foley, “Minimally Invasive Transforaminal Lumbar Interbody Fusion (TLIF),” *J. Spinal Disord. Tech.*, vol. 18, no. Supplement 1, pp. S1–S6, 2005.

[10] Y. Kawaguchi, H. Matsui, R. Gejo, and H. Tsuji, “Preventive measures of back muscle injury after posterior lumbar spine surgery in rats,” *Spine*, vol. 23, no. 21. pp. 2282–2288, 1998.

[11] K. T. Foley, L. T. Holly, and J. D. Schwender, “Minimally invasive lumbar fusion,” *Spine (Phila. Pa. 1976).*, vol. 28, no. 15S, pp. S26–S35, 2003.

[12] University of Virginia, “Minimally Invasive Spine Surgery | Neurosurgery.” [Online]. Available: https://med.virginia.edu/neurosurgery/services/spine-surgery/treatment/minimally-invasive-spine-surgery/. [Accessed: 30-Jan-2021].

[13] P. C. Hsieh *et al.*, “Maximizing the potential of minimally invasive spine surgery in complex spinal disorders,” *Neurosurg. Focus*, vol. 25, no. 2, pp. 1–10, 2008.

[14] J. A. Youssef *et al.*, “Minimally invasive surgery: Lateral approach interbody fusion: Results and review,” *Spine (Phila. Pa. 1976).*, vol. 35, no. SUPPL. 26S, pp. 302–311, 2010.

[15] J. E. O’Toole, K. M. Eichholz, and R. G. Fessler, “Surgical site infection rates after minimally invasive spinal surgery: Clinical article,” *J. Neurosurg. Spine*, vol. 11, no. 4, pp. 471–476, 2009.

[16] K. Cleary *et al.*, “Technology Improvements for Image-Guided and Minimally Invasive Spine Procedures,” *IEEE Trans. Inf. Technol. Biomed.*, vol. 6, no. 4, p. 249, 2002.

[17] M. Armen Deukmedjian, MD, Rohit Vasan, MD and Juan S. Uribe, “Minimally Invasive Spine Surgery— Who Can it Help?” [Online]. Available: https://www.practicalpainmanagement.com/treatments/interventional/minimally-invasive-spine-surgery-who-can-it-help. [Accessed: 27-Feb-2020].

[18] S. Sharif, Y. Shaikh, and N. Peev, “Minimally Invasive Spinal Surgery: How to Keep out of Trouble,” *World Neurosurg.*, vol. 119, pp. 517–526, 2018.

[19] J. A. Sclafani and C. W. Kim, “Complications Associated With the Initial Learning Curve of Minimally Invasive Spine Surgery A Systematic Review,” *Symp. Minim. INVASIVE SPINE Surg.*

[20] S. Sharif and A. Afsar, “Learning Curve and Minimally Invasive Spine Surgery,” *World Neurosurg.*, vol. 119, pp. 472–478, 2018.

[21] N. Epstein, “Learning curves for minimally invasive spine surgeries: Are they worth it?,” *Surgical Neurology International*, vol. 8, no. 1. Medknow Publications, 2017.

[22] C. H. Wong, “Comparison of Intraoperative Radiation Exposure for O-Arm Intraoperativect vs. C-Arm Image Intensifier in Minimally Invasive Lumbar Fusion,” 2017.

[23] Z. A. Smith and R. G. Fessler, “Paradigm changes in spine surgery-evolution of minimally invasive techniques,” *Nat. Rev. Neurol.*, vol. 8, pp. 443–450, 2012.

[24] A. Karhade, Vasudeva, Pompeu, and Lu, “Image Guided Spine Surgery: Available Technology and Future Potential,” *Austin Neurosurg Open Access*, vol. 3, no. 3, pp. 1043–1, 2016.

[25] L. T. Holly and K. T. Foley, “Image Guidance in Spine Surgery,” *Orthopedic Clinics of North America*, vol. 38, no. 3. pp. 451–461, 2007.

[26] W. D. Zelenty, J. R. Renehan, J. Ferguson, and F. F. Mo, “Intraoperative navigation: Current applications and future directions,” *Semin. Spine Surg.*, vol. 32, no. 2, 2020.

[27] A. Mason *et al.*, “The accuracy of pedicle screw placement using intraoperative image guidance systems: A systematic review,” *Journal of Neurosurgery: Spine*, vol. 20, no. 2. American Association of Neurological Surgeons, pp. 196–203, 01-Feb-2014.

[28] S. McClelland III and J. A. Goldstein, “Minimally Invasive versus Open Spine Surgery: What Does the Best Evidence Tell Us? Minimally invasive surgery versus conventional open surgery: Cervical disc herniation,” 2017.

[29] S. Reaungamornrat, A. S. Wang, A. Uneri, Y. Otake, A. J. Khanna, and J. H. Siewerdsen, “Deformable image registration with local rigidity constraints for cone-beam CT-guided spine surgery,” *Phys. Med. Biol.*, vol. 59, no. 14, pp. 3761–3787, Jul. 2014.

[30] T. De Silva *et al.*, “3D-2D image registration for target localization in spine surgery: investigation of similarity metrics providing robustness to content mismatch HHS Public Access,” *Phys Med Biol*, vol. 61, no. 8, pp. 3009–3025, 2016.

[31] A. Uneri *et al.*, “Intraoperative evaluation of device placement in spine surgery using known-component 3D–2D image registration,” *Phys. Med. Biol*, vol. 62, pp. 3330–3351, 2017.

[32] V. Cordemans, L. Kaminski, X. Banse, B. G. Francq, C. Detrembleur, and O. Cartiaux, “Pedicle screw insertion accuracy in terms of breach and reposition using a new intraoperative cone beam computed tomography imaging technique and evaluation of the factors associated with these parameters of accuracy: a series of 695 screws,” *Eur. Spine J.*, vol. 26, no. 11, pp. 2917–2926, Nov. 2017.

[33] M. Yang *et al.*, “Application of 3D rapid prototyping technology in posterior corrective

surgery for Lenke 1 adolescent idiopathic scoliosis patients," *Med. (United States)*, vol. 94, no. 8, p. e582, 2015.

[34] L. E. Diment, M. S. Thompson, and J. H. M. Bergmann, "Clinical efficacy and effectiveness of 3D printing: A systematic review," *BMJ Open*, vol. 7, no. 12. BMJ Publishing Group, 01-Dec-2017.

[35] M. R. Hsu, M. S. Haleem, and W. Hsu, "3D Printing Applications in Minimally Invasive Spine Surgery," *Minimally Invasive Surgery*, vol. 2018. 2018.

[36] V. S. Vasudeva, M. Abd-El-Barr, Y. A. Pompeu, A. Karhade, M. W. Groff, and Y. Lu, "Use of Intraoperative Ultrasound During Spinal Surgery," *Glob. Spine J.*, vol. 7, no. 7, pp. 648–656, Oct. 2017.

[37] M. Ganau, N. Syrmos, A. R. Martin, F. Jiang, and M. G. Fehlings, "Intraoperative ultrasound in spine surgery: history, current applications, future developments," *Quantitative Imaging in Medicine and Surgery*, vol. 8, no. 3. AME Publishing Company, pp. 261–267, 01-Apr-2018.

[38] E. Marieb and K. Hoehn, *Human anatomy & physiology*, 10th ed. Pearson, 2014.

[39] C. B. Pydi and S. Rentala, "Development of database for central nervous system (CNS) disorders and herbal remedies," *Int. J. Pharma Bio Sci.*, vol. 4, no. 1, Jan. 2013.

[40] A. Asher, "Why Do We Have Spinal Curves?," 2019. [Online]. Available: https://www.verywellhealth.com/spinal-curves-297192. [Accessed: 28-Jan-2021].

[41] P. D. Angevine and M. G. Kaiser, "RADIOGRAPHIC MEASUREMENT TECHNIQUES," *Neurosurgery*, vol. 63, no. suppl_3, pp. A40–A45, Sep. 2008.

[42] A. L. Low, C. Muller-Karger, and L. Zambrano, “Análisis de sensibilidad de las propiedades del material aplicadas a un modelo de disco intervertebral,” in *Pan American Health Care Exchanges, PAHCE*, 2013.

[43] G. Fan *et al.*, “Significant reduction of fluoroscopy repetition with lumbar localization system in minimally invasive spine surgery,” *Med. (United States)*, vol. 96, no. 21, May 2017.

[44] Z. Buser, A. S. Chung, A. Abedi, and J. C. Wang, “The future of disc surgery and regeneration,” *International Orthopaedics*, vol. 43, no. 4. Springer Verlag, pp. 995–1002, 04-Apr-2019.

[45] E. Dakwar, A. Deukmedjian, Y. Ritter, C. Dain Allred, and G. R. Rechtine, *Spinal Pathology, Conditions, and Deformities*, Second Edi. Elsevier Inc., 2016.

[46] K. Phan and R. J. Mobbs, “Minimally invasive versus open laminectomy for lumbar stenosis a systematic review and meta-analysis,” *Spine (Phila. Pa. 1976).*, vol. 41, no. 2, pp. E91–E100, 2016.

[47] “Minimally-Invasive Lumbar Microdecompression | MILM | Dr. Paul Jeffords, MD.” [Online]. Available: https://www.pauljeffordsmd.com/minimally-invasive-lumbar-microdecompression. [Accessed: 04-Jun-2021].

[48] M. R. Rasouli, V. Rahimi-Movaghar, F. Shokraneh, M. Moradi-Lakeh, and R. Chou, “Minimally invasive discectomy versus microdiscectomy/open discectomy for symptomatic lumbar disc herniation,” *Cochrane Database of Systematic Reviews*, vol. 2014, no. 9. John Wiley and Sons Ltd, 04-Sep-2014.

[49] P. Kambin and A. Vaccaro, “Arthroscopic microdiscectomy,” *Spine J.*, vol. 3, no. 3 SUPPL. 1, pp. 60–64, 2003.

[50] E. Benzel, *Spine surgery: techniques, complication avoidance, and management*. 2005.

[51] R. G. Fessler, J. E. O'Toole, K. M. Eichholz, and M. J. Perez-Cruet, "The Development of Minimally Invasive Spine Surgery," *Neurosurgery Clinics of North America*, vol. 17, no. 4. Neurosurg Clin N Am, pp. 401–409, Oct-2006.

[52] T. Stonecipher, S. W.- Spine, and undefined 1989, "Posterior lumbar interbody fusion with facet-screw fixation.," *europepmc.org*.

[53] P. V. Mummaneni and G. E. Rodts, "The mini-open transforaminal lumbar interbody fusion," *Neurosurgery*, vol. 57, no. 4 SUPPL., Oct. 2005.

[54] L. T. Holly, J. D. Schwender, D. P. Rouben, and K. T. Foley, "Minimally invasive transforaminal lumbar interbody fusion: indications, technique, and complications.," *Neurosurg. Focus*, vol. 20, no. 3, pp. 3–7, 2006.

[55] "Transforaminal Lumbar Interbody Fusion Surgery Atlanta | Spine Center." [Online]. Available: https://spinecenteratlanta.com/patient-resources/conditions/fbss/types-of-fbss/failed-spinal-fusion/failed-tlif/. [Accessed: 04-Jun-2021].

[56] M. Payer, "'Minimally invasive' lumbar spine surgery: A critical review," *Acta Neurochirurgica*, vol. 153, no. 7. Springer, pp. 1455–1459, 01-Jul-2011.

[57] J. Houten, A. T.-S. neurology international, and undefined 2011, "Comparison of postoperative values for C-reactive protein in minimally invasive and open lumbar spinal fusion surgery," *ncbi.nlm.nih.gov*.

[58] A. Kulkarni, T. Kunder, S. Das, and S. Tapashetti, "Expanding the horizons of minimally invasive spine surgery," *Indian Spine J.*, vol. 3, no. 1, p. 11, 2020.

[59] M. Y. Wang and P. V. Mummaneni, “Minimally invasive surgery for thoracolumbar spinal deformity: Initial clinical experience with clinical and radiographic outcomes,” *Neurosurg. Focus*, vol. 28, no. 3, pp. 1–8, 2010.

[60] Y. B. Kim and S. J. Hyun, “Clinical Applications of the Tubular Retractor on Spinal Disorders,” *J. Korean Neurosurg. Soc.*, vol. 42, no. 4, p. 245, 2007.

[61] J. Tehranzadeh, C. Andrews, and E. Wong, “LUMBAR SPINE IMAGING,” *Radiol. Clin. North Am.*, vol. 38, no. 6, pp. 1207–1253, Nov. 2000.

[62] G. K. Harada, Z. K. Siyaji, S. Younis, P. K. Louie, D. Samartzis, and H. S. An, “Imaging in spine surgery: Current concepts and future directions,” *Spine Surgery and Related Research*, vol. 4, no. 2. Japanese Society for Spine Surgery and Related Research, pp. 99–110, 2020.

[63] V. V. Patel, G. B. J. Andersson, S. R. Garfin, D. L. Resnick, and J. E. Block, “Utilization of CT scanning associated with complex spine surgery,” *BMC Musculoskelet. Disord.*, vol. 18, no. 1, p. 52, Dec. 2017.

[64] E. Edström, G. Burström, R. Nachabe, P. Gerdhem, and A. Elmi Terander, “A Novel Augmented-Reality-Based Surgical Navigation System for Spine Surgery in a Hybrid Operating Room: Design, Workflow, and Clinical Applications,” *Oper. Neurosurg.*, vol. 18, no. 5, pp. 496–502, May 2020.

[65] L. T. Holly and K. T. Foley, “Intraoperative Spinal Navigation,” *Spine (Phila. Pa. 1976).*, vol. 28, no. supplement, pp. S54–S61, Aug. 2003.

[66] B. Carl, M. Bopp, M. Pojskic, B. Voellger, and C. Nimsky, “Standard navigation versus intraoperative computed tomography navigation in upper cervical spine trauma,” *Int. J. Comput. Assist. Radiol. Surg.*, vol. 14, no. 1, pp. 169–182, Jan. 2019.

[67] G. M. Malham and T. Wells-Quinn, “What should my hospital buy next?—Guidelines for the acquisition and application of imaging, navigation, and robotics for spine surgery,” *J. Spine Surg.*, vol. 5, no. 1, pp. 155–165, Mar. 2019.

[68] H.-E. Gueziri, C. Santaguida, and D. Louis Collins, “The state-of-the-art in ultrasound-guided spine interventions,” *Med. Image Anal.*, vol. 65, p. 101769, 2020.

[69] C. Xiao and B. Yan, “Ultrasound-CT Registration of Vertebrae for Image-Guided Spinal Fusion Surgeries,” 2013.

[70] S. Virk and S. Qureshi, “Navigation in minimally invasive spine surgery,” *J. Spine Surg.*, vol. 5, no. S1, pp. S25–S30, Jun. 2019.

[71] R. Härtl, K. S. Lam, J. Wang, A. Korge, F. Kandziora, and L. Audigé, “Worldwide survey on the use of navigation in spine surgery,” *World Neurosurgery*, vol. 79, no. 1. Elsevier, pp. 162–172, 01-Jan-2013.

[72] U. Spetzger, A. Von Schilling, G. Winkler, J. Wahrburg, and A. König, “The past, present and future of minimally invasive spine surgery: A review and speculative outlook,” *Minim. Invasive Ther. Allied Technol.*, vol. 22, no. 4, pp. 227–241, Aug. 2013.

[73] V. Singh, L. Manchikanti, R. M. Benyamin, S. Helm, and J. A. Hirsch, “Systematic Review Percutaneous Lumbar Laser Disc Decompression: A Systematic Review of Current Evidence,” *Pain Physician*, vol. 12, pp. 573–588, 2009.

[74] G. Rahmathulla, E. W. Nottmeier, S. M. Pirris, H. Gordon Deen, and M. A. Pichelmann, “Intraoperative image-guided spinal navigation: Technical pitfalls and their avoidance,” *Neurosurg. Focus*, vol. 36, no. 3, p. 3, Mar. 2014.

[75] E. W. Nottmeier, C. Bowman, and K. L. Nelson, “Surgeon radiation exposure in cone beam

computed tomography-based, image-guided spinal surgery," *Wiley Online Libr.*, vol. 8, no. 2, pp. 196–200, Jun. 2011.

[76] E. Nottmeier, S. Pirris, S. Edwards, S. K.-… of N. Spine, and undefined 2013, "Operating room radiation exposure in cone beam computed tomography–based, image-guided spinal surgery," *thejns.org*.

[77] S. Peh *et al.*, "Accuracy of augmented reality surgical navigation for minimally invasive pedicle screw insertion in the thoracic and lumbar spine with a new tracking device," *Spine J.*, vol. 20, no. 4, pp. 629–637, Apr. 2020.

[78] C. Lee Ventola, "Medical applications for 3D printing: Current and projected uses," *P T*, vol. 39, no. 10, pp. 704–711, Oct. 2014.

[79] T. L. Gerstle, A. M. S. Ibrahim, P. S. Kim, B. T. Lee, and S. J. Lin, "A plastic surgery application in evolution: Three-dimensional printing," *Plast. Reconstr. Surg.*, vol. 133, no. 2, pp. 446–451, Feb. 2014.

[80] M. P. Chae and W. M. Rozen, "Image-Guided 3D-Printing and Haptic Modeling in Plastic Surgery The Efficiency of Microsurgical Breast Reconstruction View project 3D printing breast volumetric analysis for planning reconstruction View project."

[81] M. C. Goiato, M. R. Santos, A. A. Pesqueira, A. Moreno, D. M. dos Santos, and M. F. Haddad, "Prototyping for Surgical and Prosthetic Treatment," *J. Craniofac. Surg.*, vol. 22, no. 3, pp. 914–917, May 2011.

[82] G. T. Klein, Y. Lu, and M. Y. Wang, "3D printing and neurosurgery--ready for prime time?," *World Neurosurg.*, vol. 80, no. 3–4, pp. 233–235, Sep. 2013.

[83] M. P. Chae, W. M. Rozen, P. G. McMenamin, M. W. Findlay, R. T. Spychal, and D. J. Hunter-

Smith, “Emerging Applications of Bedside 3D Printing in Plastic Surgery,” *Front. Surg.*, vol. 2, no. June, pp. 1–14, 2015.

[84] M. Vatandsoost and S. Litkouhi, “The Future of Healthcare Facilities: How Technology and Medical Advances May Shape Hospitals of the Future,” *Hosp. Pract. Res.*, vol. 4, no. 1, pp. 1–11, 2019.

[85] J. Banks, “Adding value in additive manufacturing: Researchers in the United Kingdom and Europe look to 3D printing for customization,” *IEEE Pulse*, vol. 4, no. 6, pp. 22–26, 2013.

[86] C. Schubert, M. C. Van Langeveld, and L. A. Donoso, “Innovations in 3D printing: a 3D overview from optics to organs,” *bjo.bmj.com*.

[87] I. Ursan, L. Chiu, A. P.-J. of the A. Pharmacists, and undefined 2013, “Three-dimensional drug printing: a structured review,” *Elsevier*.

[88] G. N. Levy, R. Schindel, and J. P. Kruth, “Rapid manufacturing and rapid tooling with layer manufacturing (LM) technologies, state of the art and future perspectives,” *CIRP Ann. - Manuf. Technol.*, vol. 52, no. 2, pp. 589–609, Jan. 2003.

[89] M. B. Hoy, “3D Printing: Making Things at the Library,” *Med. Ref. Serv. Q.*, vol. 32, no. 1, pp. 93–99, Jan. 2013.

[90] W. Sealy, “ADDITIVE MANUFACTURING AS A DISRUPTIVE TECHNOLOGY: HOW TO AVOID THE PITFALL,” 2012.

[91] M. Javaid and A. Haleem, “Additive manufacturing applications in medical cases: A literature based review,” *Alexandria J. Med.*, vol. 54, no. 4, pp. 411–422, 2018.

[92] B. Gross, J. Erkal, S. Lockwood, and C. Chen, “Evaluation of 3D printing and its potential

impact on biotechnology and the chemical sciences," 2014.

[93] R. J. Barth *et al.*, "A Patient-Specific 3D-Printed Form Accurately Transfers Supine MRI-Derived Tumor Localization Information to Guide Breast-Conserving Surgery," *Ann. Surg. Oncol.*, vol. 24, no. 10, pp. 2950–2956, 2017.

[94] B. S. Ko *et al.*, "MRI-based 3D-printed surgical guides for breast cancer patients who received neoadjuvant chemotherapy," *Sci. Rep.*, vol. 9, no. 1, pp. 1–6, 2019.

[95] D. F. Redaelli, F. A. Storm, E. Biffi, G. Reni, and G. Colombo, "A Virtual Design Process to Produce Scoliosis Braces by Additive Manufacturing," vol. 1, pp. 860–870, 2020.

[96] Y. Zhang and T. H. Kwok, "Customization and topology optimization of compression casts/braces on two-manifold surfaces," *CAD Comput. Aided Des.*, vol. 111, pp. 113–122, 2019.

[97] D. Hoang, D. Perrault, M. Stevanovic, and A. Ghiassi, "Surgical applications of three-dimensional printing: A review of the current literature & how to get started," *Ann. Transl. Med.*, vol. 4, no. 23, 2016.

[98] B. Garg and N. Mehta, "Current status of 3D printing in spine surgery," *J. Clin. Orthop. Trauma*, vol. 9, pp. 218–225, 2018.

[99] E. D. Sheha, S. D. Gandhi, and M. W. Colman, "3D printing in spine surgery," *Ann. Transl. Med.*, vol. 7, no. S5, pp. S164–S164, Sep. 2019.

[100] D. POPESCU, D. ANANIA, C. AMZA, and D. CICIC, "Design and Rapid Manufacturing of patient-specific spinal surgical guides: a survey," *Proc. Manuf. Syst.*, vol. 7, no. 2, pp. 115–1, 2012.

[101] P. Tack, J. Victor, P. Gemmel, and L. Annemans, “3D-printing techniques in a medical setting: A systematic literature review,” *BioMedical Engineering Online*, vol. 15, no. 1. 2016.

[102] Y. Kawaguchi, M. Nakano, T. Yasuda, S. Seki, T. Hori, and T. Kimura, “Development of a New Technique for Pedicle Screw and Magerl Screw Insertion Using a 3-Dimensional Image Guide,” *Spine (Phila. Pa. 1976).*, vol. 37, no. 23, pp. 1983–1988, Nov. 2012.

[103] S. Lu *et al.*, “A Novel Patient-Specific Navigational Template for Cervical Pedicle Screw Placement,” *Spine (Phila. Pa. 1976).*, vol. 34, no. 26, pp. E959–E966, Dec. 2009.

[104] T. Sugawara *et al.*, “Multistep pedicle screw insertion procedure with patient-specific lamina fit-and-lock templates for the thoracic spine: Clinical article,” *J. Neurosurg. Spine*, vol. 19, no. 2, pp. 185–190, Aug. 2013.

[105] V. Ferrari *et al.*, “An optimal design for patient-specific templates for pedicle spine screws placement,” *Int. J. Med. Robot. Comput. Assist. Surg.*, vol. 9, no. 3, pp. 298–304, Sep. 2013.

[106] F. Naddeo, E. Cataldo, A. Naddeo, N. Cappetti, and N. Narciso, “An automatic and patient-specific algorithm to design the optimal insertion direction of pedicle screws for spine surgery templates,” *Med. Biol. Eng. Comput.*, vol. 55, no. 9, pp. 1549–1562, Sep. 2017.

[107] R. Bibb, D. Eggbeer, P. Evans, A. Bocca, and A. Sugar, “Rapid manufacture of custom-fitting surgical guides,” *Rapid Prototyp. J.*, vol. 15, no. 5, pp. 346–354, Sep. 2009.

[108] G. Fan *et al.*, “Significant improvement of puncture accuracy and fluoroscopy reduction in percutaneous transforaminal endoscopic discectomy with novel lumbar location system preliminary report of prospective hello study,” *Med. (United States)*, vol. 94, no. 49, 2015.

[109] S. Chakraborty *et al.*, “CAR Standard for Magnetic Resonance Imaging,” *Can. Assoc. Radiol.*, pp. 1–45, 2011.

[110] Z. Su, L. Chen, X. He, F. Yang, and L. Sass, “Planar structures with automatically generated bevel joints,” *Comput. Graph.*, vol. 72, pp. 98–105, May 2018.

[111] C. Robeller and Y. Weinand, “Interlocking folded plates-integral mechanical attachment for structural wood panels,” in *Advanced Timber Structures: Architectural Designs and Digital Dimensioning*, Birkhauser Verlag AG, 2017, pp. 200–209.

[112] N. Nestler, C. Wesemann, B. C. Spies, F. Beuer, and A. Bumann, “Dimensional accuracy of extrusion- and photopolymerization-based 3D printers: In vitro study comparing printed casts,” *J. Prosthet. Dent.*, vol. 125, no. 1, pp. 103–110, Jan. 2021.

[113] Creaform, “GO! Scan 3D.” .

[114] T. T. Kim, J. P. Johnson, R. Pashman, and D. Drazin, “Clinical Study Minimally Invasive Spinal Surgery with Intraoperative Image-Guided Navigation,” 2016.